



## Early Eocene crustal thickening in southern Tibet: New age and geochemical constraints from the Gangdese batholith

Wei-Qiang Ji <sup>a,\*</sup>, Fu-Yuan Wu <sup>a</sup>, Chuan-Zhou Liu <sup>a</sup>, Sun-Lin Chung <sup>b</sup>

<sup>a</sup> State Key Laboratory of Lithospheric Evolution, Institute of Geology and Geophysics, Chinese Academy of Sciences, P.O. Box 9825, Beijing 100029, China

<sup>b</sup> Department of Geosciences, National Taiwan University, Taipei 106, Taiwan

### ARTICLE INFO

#### Article history:

Available online 16 November 2011

#### Keywords:

Eocene  
Crustal thickening  
Gangdese batholith  
Zircon U–Pb age and Hf isotope  
Geochemistry  
Lhasa terrane  
Tibet

### ABSTRACT

The Lhasa terrane, southern Tibet is where the thickest part of the Earth's crust occurs as a result of the India–Asia collision. This paper reports zircon U–Pb age and geochemical data of samples collected from the Gangdese batholith, southern Lhasa terrane, a subset of which has already been dated at 65–41 Ma using zircon U–Pb geochronology (Ji, W.Q., Wu, F.Y., Chung, S.L., Li, J.X., Liu, C.Z., 2009a). Zircon U–Pb chronology and Hf isotopic constraints on the petrogenesis of Gangdese batholiths, southern Tibet. Chemical Geology 262, 229–245), to constrain the timing and mechanism(s) responsible for crustal thickening beneath southern Tibet. Our new data indicate that the Gangdese magmatism lasted continuously from ca. 65 to 34 Ma, during which geochemical evidence for crustal thickening is observed. Crustal thickening is best illustrated by the progressive increase in La/Yb and Sr/Y of the Early to latest Eocene magmatic rocks, associated with the decrease in Hf isotopic ratios of Paleocene to Eocene magmatic zircons. We also identify in this study the oldest (ca. 51 Ma), “post-collisional” adakitic granitoids in the Gangdese batholith, interpreted as products from partial melting of underplated basaltic lower crust. Therefore, a thickened crust likely existed by that time, at least locally, in the southern Lhasa terrane, Tibet.

© 2011 Elsevier Ltd. All rights reserved.

### 1. Introduction

The India–Asia collision and continuous northward movement of the Indian continent created the Tibetan plateau, which has the thickest crust known to date on Earth. Various models have been proposed to account for the relationship among continental convergence, crustal thickening and plateau uplift (Johnson, 2002), including distributed/homogeneous thickening (Dewey et al., 1988; England and Houseman, 1986), crustal injection (Zhao and Morgan, 1985, 1987) and underthrusting of the Indian continent (Argand, 1924; Powell and Conaghan, 1973; Powell, 1986).

In the distributed/homogeneous thickening model, the Asian and the Indian continents are regarded as viscous continuum and rigid indenter, respectively, and the Asian lithosphere had been shortened and thickened after the collision (cf. England and Houseman, 1986). However, this model appears to be oversimplified because the two continents likely possess contrasting strengths due to different thermal state and hydrous fluid contents, and that the Indian lithosphere is confined to the south of the Yarlung Tsangpo suture within the Himalaya (Johnson, 2002). In the crustal injection model, the relatively rigid Indian crust is believed to have injected into the weak Asian lower crust with low viscosity, analo-

gous to a piston displaced in a hydraulic jack (Zhao and Morgan, 1985, 1987). Because of its unusually high strength (Jackson et al., 2004, and references therein), however, the Indian crust is unlikely to be decoupled from the underlying lithospheric mantle as required in the model. Even if the Indian crust could be injected into the Asian lower crust, it would have stopped the heat supplied by the asthenospheric mantle and caused magmatism in the southern Lhasa terrane to cease, a phenomenon that is not observed. The model of underthrusting suggests that uplift of the Tibetan Plateau was caused by subduction of the Indian continent, with or without lithospheric mantle, beneath Asia (Powell and Conaghan, 1973; Powell, 1986). And a double crustal thickness is achieved by underlying of the Indian crust beneath the Asian crust from north to south, not by the progressive increasing of crustal thickness in vertical direction.

The Lhasa terrane of the Tibetan plateau is the southernmost geological unit of the Asian continent and should first be affected by continental collision. Therefore, it is an ideal region to study the effects of continental collision on crustal evolution and plateau formation. The temporal variation of crustal thickness provides important constraints on the mechanism(s) responsible for crustal thickening and plateau uplift. Occurrences of adakites in the southern Lhasa terrane are consistent with significant crustal thickening in the southern Lhasa terrane between 50–40 and 24 Ma (Mo et al., 2007) or ca. 45 and 30 Ma (Chung et al., 2009). How the crust

\* Corresponding author. Tel.: +86 10 82998439; fax: +86 10 62010846.

E-mail address: [jiweiqiang@mail.igcas.ac.cn](mailto:jiweiqiang@mail.igcas.ac.cn) (W.-Q. Ji).

thereof evolved between these times remains unclear due to sparse magmatic record from ~40 to 30 Ma.

In this study, we present zircon U-Pb geochronological, zircon Hf isotopic and whole-rock geochemical data on Paleocene–Eocene magmatic rocks of the Gangdese batholith. This comprehensive dataset enables better characterization for Paleocene–Eocene magmatism (65–34 Ma) in the southern Lhasa terrane and can be used to constrain the timing and mechanism(s) for crustal thickening.

## 2. Geological background and sample description

The Tibetan plateau comprises a series of east–west-trending blocks, from the south to the north, i.e., Himalaya, Lhasa, Qiangtang, Songpan-Ganze, and Kunlun terranes (Yin and Harrison, 2000). The Yarlung-Tsangpo suture separates Himalaya to the south and the Lhasa terrane to the north (Fig. 1a). The Lhasa terrane is a tectonomagmatic belt with a length of ~2500 km and a width ranging from <100 km to ~300 km. It is divided into the southern and northern Lhasa terranes by the Songduo eclogite belt identified recently by Yang et al. (2009), and Zhu et al. (2010, 2011) further subdivided the northern block into two parts, i.e., central and northern Lhasa terranes. Ancient basement rocks are exposed only in a limited way in the Lhasa terrane (Guynn et al., 2006; Hu et al., 2005; Xu et al., 1985). The overlying Paleozoic strata, distributed locally in the central Lhasa terrane, include Ordovician–Silurian limestones and Carboniferous–Permian volcano-sedimentary sequences (Pan et al., 2004; Zhu et al., 2010). Mesozoic–Cenozoic volcanic rocks and sedimentary sequences crop out widely in the

Lhasa terrane (Coulon et al., 1986; Pan et al., 2004), such as the Duoni Formation in the north, the Zenong Group in the central (Kang et al., 2008; Zhu et al., 2006, 2009a), the Yeba Formation, Sangri and the Linzizong Groups in the south (He et al., 2007; Lee et al., 2009; Mo et al., 2003; Zhu et al., 2008, 2009b), and the late Cretaceous Xigaze fore-arc sediments (Dürr, 1996; Einsele et al., 1994; Wu et al., 2010).

Granitic rocks are also widespread in the Tibetan plateau (Debon et al., 1986; Harris et al., 1988; Mo et al., 2005a). In particular, a huge plutonic belt, i.e., the Gangdese batholith, outcrops along the southern margin of the Lhasa terrane, which extends from the Kailas in the west to Namche Barwa in the east (Fig. 1a). It constitutes the prominent part of the Transhimalayan Batholith, which has a total length over 3000 km and stretches from Kohistan–Ladakh batholith in the west through Gangdese batholith in the middle to the Chayu–Dianxi–Burma batholith in the east (Ji et al., 2009a). Previous study has suggested that the Gangdese batholith was active from mid-Cretaceous to Eocene (Schäfer et al., 1984). However, recent studies revealed that the Gangdese batholith has a longer magmatic history lasting from Late Triassic to Miocene, with a peak at Paleocene–Eocene (Chu et al., 2006; Chung et al., 2003; Dong et al., 2005; Hou et al., 2004; Ji et al., 2009a; Mo et al., 2005b; Quidelleur et al., 1997; Wen et al., 2008a,b; Zhang et al., 2010a), whereas age spectrum of detrital zircons from Xigaze Group suggests two earlier magmatic peaks, i.e., late Jurassic (ca. 170–150 Ma) and early Cretaceous (ca. 125–100 Ma) (Wu et al., 2010). Various lithologies, including gabbro, diorite, granodiorite, monzogranite, and syenogranite, are

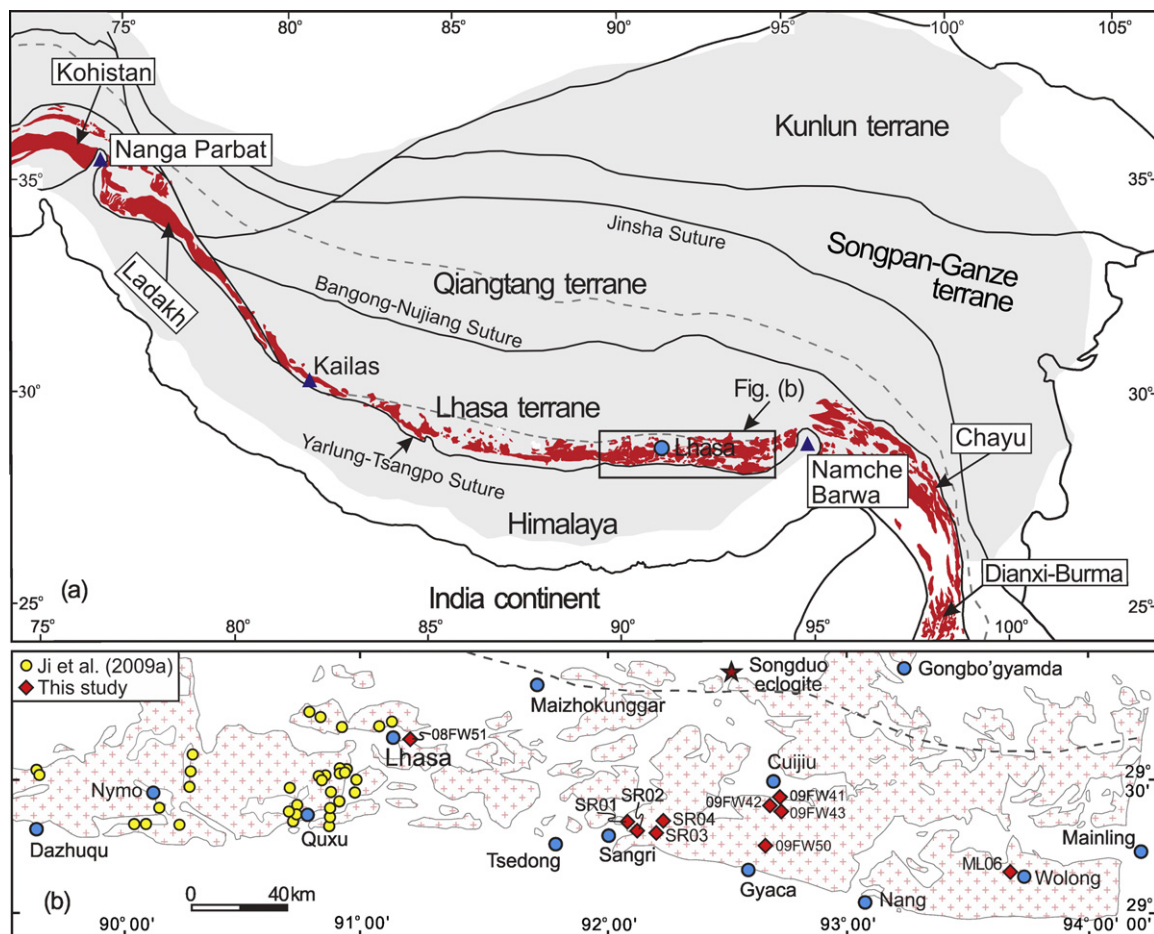


**Fig. 1.** (a) Simplified tectonic sketch map showing the distribution of the Transhimalayan batholiths. (b) Distribution map of Paleocene–Eocene samples between Dazhuqu and Mainling with sample number labeled for the newly dated samples from Lhasa–Mainling segment.

outcropped in the Gangdese batholith, which commonly contain hornblende and/or biotite. Therefore, the majority of the Gangdese batholith belongs to I-type granitoids (Chappell and White, 1974; Debon et al., 1986; Harris et al., 1988).

In this study, we presented whole-rock compositions of 33 samples from the Lhasa–Dazhuqu segment, which have been previously dated to have Paleocene–Eocene ages (65–41 Ma; Ji et al., 2009a). Furthermore, we have conducted abundant analyses on samples from the Lhasa–Mainling segment of Gangdese batholith (Ji, 2010), and found that a small amount of granitoids yielded Paleocene–Eocene ages (i.e., ten out of over 100 samples). Here we supplement the whole rock compositions, zircon U–Pb ages and Hf isotopes of these ten samples, which comprise of six granodiorites, three monzogranites and one granite. These ten samples are medium to coarse-grained and contain quartz, plagioclase, K-feldspar, hornblende and biotite, but minor apatite, sphene and zircon.

The zircon U–Pb and Hf isotopic compositions were determined simultaneously at the MC-ICPMS of the Institute of Geology and Geophysics, Chinese Academy of Sciences (IGGCAS). The detailed

procedure has been described in Xie et al. (2008). Major elements were measured by XRF method at IGGCAS. Trace elements were analyzed by ICPMS at IGGCAS and China University of Geosciences (Wuhan), following the method of Liu et al. (2008).

### 3. Analytical results

The zircon U–Pb and Lu–Hf isotopic data are listed in the supplementary Tables A.1 and A.2, respectively and summarized in Table 1. The whole rock compositions are given in Table 2.

#### 3.1. Zircon U–Pb ages

The separated zircons are euhedral and show long or short prismatic forms, with crystal lengths of ~80–250 µm and length-to-width ratios ranging from 1:1 to 4:1. They are transparent in color and possess oscillatory zoning. Their Th/U ratios are larger than 0.15, with most larger than 0.5 (Table A.1). All these characteristics

**Table 1**

Summary of zircon U–Pb age and Hf isotope analytical results for the Paleocene–Eocene Gangdese batholith (Dazhuqu–Mainling segment).

Sample	Long. (°E)	Lat. (°N)	Location	Rock type	SiO <sub>2</sub> (wt.%)	Age(Ma)	<sup>176</sup> Lu/ <sup>177</sup> Hf	<sup>176</sup> Hf/ <sup>177</sup> Hf	$\varepsilon_{\text{Hf}}(t)$
<i>Lhasa–Milin segment</i>									
08FW51	91.164	29.637	Southeast of Lhasa	Granodiorite	66.35	64.5 ± 2.3	0.001081	0.283035 ± 11	10.7 ± 0.4
SR01-1	92.096	29.288	Sangri	Granodiorite	62.52	45.4 ± 0.7	0.000650	0.283004 ± 10	9.2 ± 0.4
SR02-1	92.119	29.288	Sangri	Granite	72.05	37.7 ± 0.7	0.000910	0.282926 ± 23	6.2 ± 0.8
SR03-1	92.217	29.267	Zangga	Granodiorite	71.48	59.8 ± 0.9	0.001730	0.282960 ± 13	7.9 ± 0.5
SR04-1	92.237	29.316	Woka	Granodiorite	61.81	42.1 ± 0.7	0.001380	0.282965 ± 7	7.7 ± 0.2
09FW41	92.738	29.419	Cuijiu	Monzogranite	70.44	56.1 ± 1.1	0.001147	0.283010 ± 10	9.6 ± 0.4
09FW42	92.745	29.407	Cuijiu	Monzogranite	69.74	50.7 ± 1.1	0.000810	0.282947 ± 9	7.3 ± 0.3
09FW43	92.745	29.407	Cuijiu	Monzogranite	70.66	42.0 ± 0.7	0.000849	0.282942 ± 7	6.9 ± 0.3
09FW50	92.697	29.239	North of Jiacha	Granodiorite	67.85	50.2 ± 1.9	0.000686	0.282990 ± 7	8.8 ± 0.3
ML06-1	93.679	29.154	Wolong	Granodiorite	65.72	34.9 ± 0.4	0.001097	0.282970 ± 13	7.8 ± 0.5
LS5 <sup>a</sup>	–	–	East of Lhasa	Diorite	56.09	61.0 ± 2.9	0.001163	0.283006 ± 9	9.6 ± 0.3
<i>Lhasa–Dazhuqu segment</i>									
06FW101 <sup>b</sup>	91.112	29.687	North of Lhasa	Monzogranite	72.29	64.7 ± 1.1	0.001588	0.282956 ± 10	7.9 ± 0.3
06FW104 <sup>b</sup>	91.076	29.675	North of Lhasa	Monzogranite	71.71	64.4 ± 0.9	0.001075	0.282928 ± 23	6.9 ± 0.8
06FW105 <sup>b</sup>	90.932	29.682	Yangda	Monzogranite	67.62	55.2 ± 1.5	0.000679	0.282910 ± 12	6.0 ± 0.4
06FW108 <sup>b</sup>	90.776	29.759	North of Gurong	Granodiorite	62.25	56.8 ± 0.7	0.001320	0.282956 ± 14	7.7 ± 0.5
06FW110 <sup>b</sup>	90.833	29.738	Zhongduiguo	Monzogranite	73.45	54.3 ± 0.9	0.000903	0.282956 ± 12	7.7 ± 0.4
06FW111 <sup>b</sup>	90.956	29.443	Caina	Monzogranite	66.49	50.6 ± 0.7	0.000899	0.283054 ± 11	11.1 ± 0.4
06FW112 <sup>b</sup>	90.961	29.491	North of Caina	Granodiorite	60.23	53.4 ± 1.0	0.000836	0.283039 ± 12	10.6 ± 0.4
06FW118 <sup>b</sup>	90.939	29.499	Niedang	Monzogranite	73.27	51.0 ± 0.7	0.001013	0.283044 ± 15	10.6 ± 0.5
06FW119 <sup>b</sup>	90.939	29.499	Niedang	Granodiorite	63.91	51.2 ± 0.7	0.000910	0.283066 ± 10	11.1 ± 0.4
06FW120 <sup>b</sup>	90.939	29.499	Niedang	Dioritic enclave	51.94	50.3 ± 0.6	0.000736	0.283050 ± 12	10.9 ± 0.4
06FW121 <sup>b</sup>	90.939	29.499	Niedang	Granitic dike	75.29	51.1 ± 0.7	0.001387	0.283063 ± 20	11.0 ± 1.0
06FW126 <sup>b</sup>	90.874	29.482	Nanmu Power Station	Granodiorite	56.62	55.3 ± 1.0	0.001158	0.282919 ± 19	6.4 ± 0.7
06FW127 <sup>b</sup>	90.874	29.482	Nanmu Power Station	Granitic dike	77.16	49.5 ± 0.6	0.001279	0.282951 ± 7	7.4 ± 0.3
06FW128 <sup>b</sup>	90.874	29.482	Nanmu Power Station	Doleritic dike	54.99	49.9 ± 1.0	0.000988	0.283008 ± 39	9.4 ± 1.4
06FW129 <sup>b</sup>	90.897	29.464	Nanmu	Granodiorite	57.43	52.9 ± 0.7	0.000917	0.282916 ± 17	6.2 ± 0.6
06FW131 <sup>b</sup>	90.906	29.408	Jiangcun	Tonalitic gneiss	69.90	44.0 ± 0.8	0.000438	0.282821 ± 34	2.7 ± 1.2
06FW133 <sup>b</sup>	90.866	29.334	Galashan tunnel	Monzonite	67.45	47.1 ± 1.0	0.000421	0.282769 ± 17	0.9 ± 0.6
06FW134 <sup>b</sup>	90.876	29.361	Galashan tunnel	Monzogranite	70.57	41.9 ± 0.6	0.000446	0.282810 ± 16	2.3 ± 0.6
06FW139 <sup>b</sup>	90.882	29.383	East of Qushui	Monzonite	61.01	41.5 ± 0.7	0.000135	0.282764 ± 15	0.6 ± 0.5
06FW140 <sup>b</sup>	90.716	29.473	Badi	Monzogranite	70.99	43.7 ± 0.9	0.000347	0.282932 ± 58	7.0 ± 2.0
06FW146 <sup>b</sup>	90.718	29.403	Qupu	Monzodiorite	52.88	56.9 ± 1.4	0.000737	0.283104 ± 7	13.0 ± 0.3
06FW147 <sup>b</sup>	90.724	29.368	Northwest of Qushui	Granodiorite	61.42	51.5 ± 0.8	0.000639	0.283119 ± 9	13.4 ± 0.3
06FW148 <sup>b</sup>	90.724	29.368	Northwest of Qushui	Syenogranitic dike	71.69	51.3 ± 0.6	0.000883	0.283071 ± 14	11.7 ± 0.5
06FW151 <sup>b</sup>	90.717	29.358	West of Qushui	Diorite	56.09	55.5 ± 1.2	0.000693	0.283097 ± 11	12.7 ± 0.4
06FW152-2 <sup>b</sup>	90.179	29.401	East of Qulin	Diorite	53.49	57.3 ± 0.9	0.000500	0.283101 ± 10	12.9 ± 0.4
06FW154 <sup>b</sup>	90.274	29.578	Angang	Syenogranite	75.43	51.3 ± 0.7	0.001596	0.282974 ± 11	8.2 ± 0.4
06FW155 <sup>b</sup>	90.273	29.543	Angang Power Station	Monzodiorite	70.33	61.1 ± 1.2	0.001264	0.282955 ± 20	7.7 ± 0.7
06FW156 <sup>b</sup>	90.271	29.499	Kongdonglang	Monzodiorite	67.99	55.4 ± 0.8	0.001128	0.282979 ± 14	8.5 ± 0.5
06FW162 <sup>b</sup>	89.623	29.539	Numa	Granodiorite	60.29	50.9 ± 0.8	0.000959	0.283054 ± 11	11.8 ± 0.6
06FW163 <sup>b</sup>	89.623	29.539	Numa	Monzogranite	71.58	48.2 ± 0.7	0.000916	0.283074 ± 16	11.0 ± 0.4
06FW174 <sup>b</sup>	90.097	29.351	Karu	Diorite	56.45	50.2 ± 1.5	0.000801	0.283049 ± 11	10.9 ± 0.4
06FW175 <sup>b</sup>	90.067	29.349	Karu	Diorite	57.57	52.6 ± 1.2	0.001092	0.283061 ± 18	11.2 ± 0.6
06FW176 <sup>b</sup>	90.249	29.335	Nimu	Diorite	54.48	53.6 ± 1.0	0.001458	0.283601 ± 25	11.3 ± 0.9
RB12 <sup>b</sup>	–	–	Renbu	Diorite	54.73	45.0 ± 1.6	0.000535	0.283048 ± 10	10.7 ± 0.3
LS2 <sup>b</sup>	–	–	North of Lhasa	Syenogranite	69.59	51.0 ± 1.2	0.001294	0.282835 ± 20	3.3 ± 0.7

<sup>a</sup> Data from Huang et al. (2010).

<sup>b</sup> Data from Ji et al. (2009a).

**Table 2**

Major and trace element data for rocks from the Paleocene–Eocene Gangdese batholith (Dazhuqu–Mainling segment).

Sample	06FW101	06FW104	06FW105	06FW108	06FW110	06FW111	06FW112	06FW118	06FW119	06FW120	06FW121
Age(Ma)	64.7	64.4	55.2	56.8	54.3	50.6	53.4	51.0	51.2	50.3	51.1
(wt.%)											
SiO <sub>2</sub>	72.29	71.71	67.62	62.25	73.45	66.49	60.23	73.27	63.91	51.94	75.29
TiO <sub>2</sub>	0.27	0.37	0.56	0.75	0.22	0.50	0.66	0.24	0.67	1.43	0.13
Al <sub>2</sub> O <sub>3</sub>	14.28	14.26	14.99	15.62	13.54	15.10	17.15	13.53	15.92	17.25	12.73
TFe <sub>2</sub> O <sub>3</sub>	1.99	2.52	3.50	6.23	1.74	4.32	6.65	1.75	5.51	10.47	1.16
MnO	0.05	0.08	0.06	0.10	0.04	0.08	0.12	0.03	0.09	0.18	0.01
MgO	0.57	0.83	1.27	2.71	0.42	1.69	2.91	0.54	2.32	3.87	0.29
CaO	2.24	2.32	3.14	5.17	1.78	3.71	6.39	1.76	4.65	8.10	1.43
Na <sub>2</sub> O	4.13	4.00	3.48	3.21	3.18	3.84	3.90	2.90	3.64	4.21	2.60
K <sub>2</sub> O	3.62	3.28	4.25	2.90	4.81	3.30	1.85	5.22	3.21	1.52	5.26
P <sub>2</sub> O <sub>5</sub>	0.07	0.10	0.16	0.16	0.05	0.16	0.19	0.05	0.19	0.48	0.03
LOI	0.33	0.45	0.37	0.37	0.55	0.68	0.43	0.35	0.48	0.55	0.40
A/CNK	0.97	0.99	0.93	0.88	0.99	0.91	0.86	0.99	0.89	0.74	1.01
Mg#	36	39	42	46	32	44	46	38	46	42	33
(ppm)											
Sc	4.35	4.90	6.82	12.88	4.30	6.81	11.93	3.99	10.93	25.54	0.32
V	23.53	31.73	54.85	119.18	19.93	81.57	151.34	26.56	124.42	267.94	26.93
Cr	2.66	1.84	9.17	20.89	1.59	9.95	13.31	3.36	19.20	0.35	1.09
Co	2.50	3.56	7.24	16.42	2.62	10.20	15.46	3.38	14.97	26.09	2.69
Ni	1.85	1.09	5.14	11.86	1.25	5.85	7.23	2.39	10.53	5.04	1.06
Cu	1.62	1.69	4.20	24.43	3.56	6.71	27.82	4.36	13.31	220.41	5.81
Zn	24.47	32.84	42.89	69.43	20.24	44.90	64.66	21.50	62.11	113.99	13.96
Ga	14.45	14.57	15.97	17.00	13.39	15.91	17.15	11.04	15.86	19.32	9.48
Rb	100	93	154	91	202	66	20	131	119	34	120
Sr	197	201	315	332	143	324	386	229	476	627	371
Y	27.16	23.78	21.38	20.03	29.89	11.32	24.55	6.70	13.10	15.16	1.54
Zr	108	171	171	164	132	187	98	115	179	72	98
Nb	9.11	9.08	10.33	6.82	9.18	5.81	7.08	2.75	5.19	9.21	0.68
Cs	3.08	3.52	9.03	9.31	9.11	4.52	3.54	4.96	6.16	1.41	3.14
Ba	415	523	661	497	380	454	370	555	690	359	1438
La	29.70	28.80	40.23	23.91	24.80	20.80	15.45	13.63	17.44	28.96	4.42
Ce	58.95	52.66	74.76	48.46	50.82	37.50	31.82	25.88	33.38	55.28	5.51
Pr	6.90	6.54	8.17	5.70	5.90	4.08	4.69	2.79	3.80	6.64	0.48
Nd	25.45	24.04	29.49	21.63	22.90	13.96	19.25	10.16	13.98	25.64	1.48
Sm	4.86	4.48	5.00	4.31	4.63	2.41	4.24	1.79	2.93	5.14	0.22
Eu	0.78	0.78	1.09	1.01	0.61	0.71	1.02	0.61	0.83	1.34	0.30
Gd	4.26	3.96	4.21	3.95	4.23	2.06	3.97	1.41	2.41	3.98	0.21
Tb	0.69	0.61	0.61	0.59	0.70	0.30	0.63	0.21	0.37	0.56	0.03
Dy	4.46	4.04	3.84	3.65	4.87	1.90	4.16	1.20	2.13	2.81	0.18
Ho	0.92	0.81	0.74	0.71	0.98	0.39	0.87	0.23	0.45	0.55	0.04
Er	2.70	2.39	2.13	1.97	2.94	1.15	2.49	0.61	1.21	1.37	0.16
Tm	0.44	0.38	0.33	0.29	0.48	0.19	0.38	0.10	0.19	0.21	0.03
Yb	3.19	2.76	2.44	1.96	3.64	1.45	2.66	0.68	1.26	1.45	0.28
Lu	0.46	0.42	0.36	0.29	0.52	0.23	0.38	0.11	0.21	0.24	0.06
Hf	3.37	4.66	4.54	4.24	4.69	4.73	2.43	3.42	4.68	1.80	3.01
Ta	0.87	0.77	0.92	0.54	1.21	0.51	0.49	0.16	0.40	1.07	0.06
Pb	13.82	10.91	25.90	21.04	15.51	11.52	13.27	14.75	13.70	10.13	14.17
Th	15.70	12.33	36.36	13.36	34.40	18.11	4.98	29.49	11.35	7.03	10.75
U	4.03	2.63	7.82	3.03	7.97	4.00	1.45	5.41	2.74	1.86	2.40
δEu	0.51	0.56	0.71	0.74	0.42	0.95	0.75	1.14	0.93	0.88	4.29
Sr/Y	7.2	8.4	14.7	16.6	4.8	28.7	15.7	34.2	36.4	41.3	241.7
La/Yb	9.3	10.4	16.5	12.2	6.8	14.3	5.8	20.0	13.8	19.9	15.5
(La/Yb) <sub>N</sub>	6.3	7.0	11.1	8.2	4.6	9.6	3.9	13.5	9.3	13.4	10.5
(Yb) <sub>N</sub>	15.3	13.2	11.7	9.4	17.4	7.0	12.7	3.3	6.1	6.9	1.4
Sample	06FW126	06FW127	06FW128	06FW129	06FW131	06FW133	06FW134	06FW139	06FW140	06FW146	06FW147
(wt.%)											
Age(Ma)	55.3	49.5	49.9	52.9	44.0	47.1	41.9	41.5	43.7	56.9	51.5
SiO <sub>2</sub>	56.62	77.16	54.99	57.43	69.90	67.45	70.57	61.01	70.99	52.88	61.42
TiO <sub>2</sub>	1.15	0.09	0.76	1.05	0.28	0.41	0.28	1.27	0.25	0.77	0.71
Al <sub>2</sub> O <sub>3</sub>	18.46	12.14	17.12	18.67	15.28	15.39	14.41	16.40	14.97	19.06	16.83
TFe <sub>2</sub> O <sub>3</sub>	6.91	0.65	8.80	6.24	2.14	2.83	1.97	5.27	1.89	9.41	6.18
MnO	0.12	0.01	0.20	0.11	0.04	0.05	0.04	0.08	0.05	0.16	0.11
MgO	2.65	0.06	4.43	2.32	0.71	1.19	0.68	2.07	0.54	4.35	2.66
CaO	5.67	0.68	7.03	5.27	2.22	2.72	1.90	4.10	1.99	8.37	5.34
Na <sub>2</sub> O	4.71	2.30	3.83	4.73	4.23	4.25	4.00	4.09	4.10	3.88	4.18
K <sub>2</sub> O	2.36	5.86	1.66	2.71	4.16	4.60	4.74	4.50	4.16	0.55	2.46
P <sub>2</sub> O <sub>5</sub>	0.42	0.01	0.20	0.37	0.12	0.21	0.13	0.82	0.10	0.34	0.22
LOI	0.60	0.40	1.18	0.60	0.73	0.67	0.62	1.00	0.38	-0.05	0.45
A/CNK	0.90	1.07	0.82	0.92	0.99	0.91	0.95	0.86	1.01	0.86	0.87
Mg#	43	15	50	42	40	46	41	44	36	48	46

(continued on next page)

**Table 2** (continued)

Sample	06FW101	06FW104	06FW105	06FW108	06FW110	06FW111	06FW112	06FW118	06FW119	06FW120	06FW121
Age(Ma)	64.7	64.4	55.2	56.8	54.3	50.6	53.4	51.0	51.2	50.3	51.1
<i>(ppm)</i>											
Sc	11.79	0.18	22.34	10.50	3.36	5.00	3.02	7.44	3.28	12.73	12.26
V	128.44	11.10	220.48	112.71	33.85	56.87	35.97	91.60	29.17	189.90	132.75
Cr	12.24	1.06	12.09	10.10	3.46	15.07	7.50	17.13	1.87	16.67	12.79
Co	14.03	0.48	25.89	12.43	4.12	7.00	4.25	11.66	3.38	24.56	16.48
Ni	7.69	1.07	9.43	6.46	3.46	9.25	5.09	9.60	2.10	12.01	9.15
Cu	26.05	3.86	40.28	21.87	26.09	4.31	5.79	36.83	21.99	23.17	45.77
Zn	96.08	7.69	102.23	91.11	35.33	32.54	44.14	116.16	45.57	89.93	73.56
Ga	20.62	7.65	17.81	20.24	17.33	19.29	18.33	24.30	17.09	18.16	16.60
Rb	78	103	106	65	225	289	302	216	181	4	58
Sr	919	603	591	942	454	568	434	874	417	865	559
Y	31.13	1.32	19.11	25.33	7.28	11.59	7.52	14.82	9.53	13.54	18.78
Zr	378	145	90	339	135	207	135	411	115	30	173
Nb	15.70	1.08	6.89	13.52	7.18	14.62	11.13	20.24	8.21	1.39	5.22
Cs	5.22	2.23	13.04	2.74	18.71	43.54	29.60	13.79	6.09	0.24	4.68
Ba	850	3084	223	1273	632	752	617	943	750	200	452
La	45.68	4.77	13.80	42.50	27.26	52.92	45.51	136.48	23.07	9.61	17.44
Ce	97.73	7.18	28.64	90.86	49.16	100.03	75.36	283.36	43.32	22.75	36.84
Pr	12.27	0.60	3.63	11.70	5.05	10.57	7.16	31.47	4.74	3.17	4.75
Nd	46.95	1.91	14.67	44.89	17.18	34.95	22.51	102.59	16.21	13.42	17.98
Sm	8.95	0.28	3.54	8.53	2.80	5.74	3.38	13.90	2.78	3.37	4.13
Eu	2.08	0.43	1.01	2.08	0.65	1.05	0.69	2.41	0.60	1.29	1.01
Gd	6.70	0.24	3.10	6.19	1.90	3.72	2.25	8.21	1.91	2.85	3.40
Tb	0.96	0.03	0.50	0.88	0.24	0.44	0.26	0.84	0.27	0.43	0.54
Dy	5.34	0.17	3.00	4.69	1.22	2.12	1.31	3.55	1.46	2.35	2.95
Ho	1.07	0.04	0.66	0.93	0.23	0.38	0.23	0.53	0.29	0.51	0.66
Er	2.87	0.14	1.84	2.44	0.60	0.99	0.64	1.26	0.80	1.30	1.81
Tm	0.45	0.03	0.29	0.37	0.09	0.15	0.09	0.15	0.13	0.19	0.28
Yb	3.10	0.28	1.90	2.25	0.66	0.97	0.68	0.85	0.92	1.20	1.79
Lu	0.48	0.05	0.31	0.34	0.10	0.15	0.11	0.12	0.14	0.19	0.29
Hf	8.82	5.15	2.54	8.02	3.83	5.82	4.01	10.29	3.65	0.88	4.79
Ta	1.11	0.07	0.54	0.88	0.72	1.53	1.20	1.01	0.98	0.08	0.37
Pb	10.04	18.11	11.51	10.12	52.53	47.56	65.44	31.15	36.03	4.84	17.61
Th	10.16	4.08	4.44	6.82	29.28	65.79	41.98	41.72	20.42	0.42	4.71
U	2.69	1.81	1.74	1.97	7.15	7.47	8.10	6.69	4.20	0.16	1.63
δEu	0.79	5.01	0.91	0.84	0.81	0.65	0.72	0.64	0.76	1.24	0.80
Sr/Y	29.5	455.6	30.9	37.2	62.3	49.1	57.7	59.0	43.7	63.9	29.8
La/Yb	14.8	17.3	7.3	18.9	41.2	54.7	67.0	161.2	25.0	8.0	9.7
(La/Yb) <sub>N</sub>	9.9	11.7	4.9	12.7	27.8	36.9	45.2	108.7	16.8	5.4	6.6
(Yb) <sub>N</sub>	14.8	1.3	9.1	10.8	3.2	4.6	3.2	4.1	4.4	5.7	8.6
Sample	06FW148	06FW151	06FW152-2	06FW154	06FW155	06FW156	06FW162	06FW163	06FW174	06FW175	06FW176
<i>(wt.%)</i>											
Age(Ma)	51.3	55.5	57.3	51.3	61.1	55.4	48.2	50.9	50.2	52.6	53.6
SiO <sub>2</sub>	71.69	56.09	53.49	75.43	70.33	67.99	60.29	71.58	56.45	57.57	54.48
TiO <sub>2</sub>	0.26	1.08	1.32	0.23	0.41	0.46	0.72	0.48	0.79	0.78	1.03
Al <sub>2</sub> O <sub>3</sub>	14.23	17.43	17.36	12.37	14.28	15.40	16.78	14.33	17.45	17.59	17.99
TFe <sub>2</sub> O <sub>3</sub>	2.17	8.40	9.18	1.71	2.02	3.28	7.01	2.88	7.84	7.24	8.47
MnO	0.06	0.14	0.15	0.05	0.05	0.06	0.12	0.04	0.15	0.14	0.15
MgO	0.71	3.48	4.08	0.32	0.89	1.11	3.24	0.80	3.06	3.06	3.09
CaO	2.33	7.22	7.66	1.17	2.52	2.79	5.11	1.73	6.93	6.56	6.97
Na <sub>2</sub> O	4.05	3.79	3.49	3.28	3.40	3.69	3.47	3.02	4.02	3.90	4.34
K <sub>2</sub> O	3.66	1.94	1.45	4.52	5.06	4.78	2.12	4.79	2.14	2.07	2.06
P <sub>2</sub> O <sub>5</sub>	0.10	0.51	0.45	0.05	0.13	0.14	0.16	0.10	0.25	0.30	0.39
LOI	0.45	0.42	0.73	0.23	0.58	0.55	0.52	0.18	0.30	0.20	0.38
A/CNK	0.96	0.81	0.82	1.00	0.91	0.94	0.97	1.08	0.81	0.85	0.82
Mg#	39	45	47	27	47	40	48	35	44	46	42
<i>(ppm)</i>											
Sc	2.76	15.45	20.52	3.41	5.12	6.15	17.45	6.91	8.65	18.67	4.84
V	37.42	160.39	240.36	15.96	30.34	58.17	172.50	151.87	182.95	159.80	50.81
Cr	5.47	32.53	26.59	1.03	6.44	8.12	4.71	10.55	4.66	10.94	1.94
Co	4.29	20.23	24.71	1.69	5.88	5.81	18.19	16.02	19.08	19.29	4.46
Ni	2.77	14.91	12.23	0.97	2.28	3.38	4.03	6.66	5.72	11.38	1.99
Cu	21.85	57.01	6.21	4.54	9.56	3.24	43.84	18.95	59.81	56.12	6.41
Zn	38.05	78.68	94.98	19.62	24.39	30.62	79.90	77.94	81.43	72.59	34.10
Ga	14.65	16.89	17.76	12.11	13.32	15.16	20.42	17.27	20.15	17.62	14.23
Rb	81	56	43	206	168	173	79	146	42	14	10
Sr	456	580	690	122	306	366	452	245	677	542	515
Y	7.01	20.82	24.34	32.50	17.16	17.69	26.01	15.12	34.08	18.02	29.67
Zr	96	121	150	119	127	150	138	345	160	82	205
Nb	4.95	5.33	8.33	16.60	11.30	10.61	8.90	9.20	7.87	5.10	7.34
Cs	2.41	2.96	7.31	8.18	7.52	6.20	6.56	2.79	2.28	2.32	1.07
Ba	681	503	501	189	563	665	517	937	370	264	230

**Table 2** (continued)

Sample	06FW101	06FW104	06FW105	06FW108	06FW110	06FW111	06FW112	06FW118	06FW119	06FW120	06FW121
Age(Ma)	64.7	64.4	55.2	56.8	54.3	50.6	53.4	51.0	51.2	50.3	51.1
La	27.30	17.74	17.62	20.76	32.71	33.81	22.08	17.48	24.73	14.18	21.28
Ce	47.17	40.89	40.56	48.90	61.54	60.68	47.84	35.97	63.59	31.12	49.25
Pr	4.79	5.26	5.35	6.43	6.46	5.83	4.31	8.69	4.59	7.92	
Nd	15.32	20.16	21.83	23.85	20.83	20.82	23.06	17.65	37.20	19.60	34.77
Sm	2.50	4.72	5.25	5.58	3.66	3.90	4.81	3.42	8.04	4.29	7.53
Eu	0.62	1.22	1.46	0.49	0.80	0.86	1.05	0.88	1.66	1.17	1.67
Gd	1.75	3.90	4.51	4.36	2.87	3.04	4.38	3.00	6.86	3.73	6.27
Tb	0.22	0.60	0.72	0.76	0.43	0.46	0.68	0.44	1.01	0.57	0.93
Dy	1.14	3.35	4.02	4.47	2.52	2.64	4.45	2.86	6.34	3.57	5.75
Ho	0.22	0.75	0.89	1.01	0.54	0.58	0.93	0.55	1.25	0.72	1.15
Er	0.60	2.00	2.38	2.97	1.57	1.63	2.65	1.56	3.46	2.00	3.17
Tm	0.09	0.32	0.36	0.53	0.27	0.28	0.42	0.23	0.51	0.31	0.46
Yb	0.64	1.99	2.23	3.75	1.88	1.87	2.96	1.66	3.36	2.04	3.04
Lu	0.10	0.33	0.37	0.61	0.32	0.32	0.44	0.25	0.47	0.30	0.44
Hf	2.72	3.45	4.37	3.86	3.61	4.22	3.77	8.88	4.44	2.12	4.79
Ta	0.41	0.39	0.56	2.02	1.07	0.99	0.79	0.50	0.43	0.28	0.29
Pb	26.21	13.33	16.44	12.15	12.50	11.71	14.40	16.29	11.30	10.74	7.57
Th	12.61	4.19	6.17	18.03	25.38	18.64	11.11	3.63	9.77	2.65	3.23
U	2.11	1.30	1.67	5.09	5.63	5.07	3.57	1.21	2.18	0.69	1.09
δEu	0.86	0.85	0.90	0.29	0.73	0.74	0.69	0.82	0.67	0.87	0.72
Sr/Y	65.0	27.9	28.3	3.8	17.8	20.7	17.4	16.2	19.9	30.1	17.4
La/Yb	42.5	8.9	7.9	5.5	17.4	18.1	7.5	10.5	7.4	6.9	7.0
(La/Yb) <sub>N</sub>	28.7	6.0	5.3	3.7	11.7	12.2	5.0	7.1	5.0	4.7	4.7
(Yb) <sub>N</sub>	3.1	9.5	10.7	17.9	9.0	8.9	14.2	8.0	16.1	9.8	14.6
Sample	08FW51	SR01-1	SR02-1	SR03-1	SR04-1	09FW41	09FW42	09FW43	09FW50	ML06-1	
(wt.%)											
Age(Ma)	64.5	45.4	37.7	59.8	42.1	56.1	50.7	42.0	50.2	34.9	
SiO <sub>2</sub>	66.35	62.52	72.05	71.48	61.81	70.44	69.74	70.66	67.85	65.72	
TiO <sub>2</sub>	0.56	0.57	0.21	0.24	0.59	0.40	0.31	0.32	0.40	0.39	
Al <sub>2</sub> O <sub>3</sub>	15.31	15.54	14.88	14.79	17.04	14.91	14.99	14.76	15.31	17.09	
TFe <sub>2</sub> O <sub>3</sub>	4.69	4.91	1.91	2.71	5.86	2.91	2.93	2.62	3.93	3.27	
MnO	0.06	0.07	0.05	0.08	0.11	0.06	0.05	0.05	0.07	0.07	
MgO	1.97	2.11	0.59	0.74	2.24	0.84	0.99	0.95	1.63	1.24	
CaO	4.38	3.87	1.75	2.92	4.64	2.20	2.35	2.56	3.49	3.65	
Na <sub>2</sub> O	3.12	3.13	4.01	4.03	4.05	3.95	3.51	3.61	3.62	5.19	
K <sub>2</sub> O	2.80	4.00	3.82	2.55	2.49	4.08	4.69	4.07	3.44	2.61	
P <sub>2</sub> O <sub>5</sub>	0.13	0.18	0.09	0.10	0.24	0.12	0.11	0.11	0.12	0.21	
LOI	0.82	3.20	0.58	0.36	1.08	0.22	0.36	0.26	0.36	0.70	
A/CNK	0.95	0.94	1.07	1.01	0.96	1.00	0.99	0.98	0.95	0.95	
Mg#	45	46	38	35	43	36	40	42	45	43	
(ppm)											
Sc	12.8	10.6	2.84	3.40	9.63	6.17	5.96	5.47	7.43	4.90	
V	106	97.3	23.9	30.5	89.4	41.4	49.4	44.5	72.2	71.6	
Cr	20.6	21.9	0.92	1.32	2.99	2.32	6.86	5.11	9.30	5.45	
Co	11.8	12.6	2.74	4.63	12.4	4.48	5.62	4.67	9.94	7.12	
Ni	10.1	10.4	1.04	1.51	3.75	2.06	3.02	2.78	6.98	5.41	
Cu	63.9	9.22	9.59	12.9	22.1	3.09	3.80	9.99	20.9	23.6	
Zn	48.9	52.0	32.4	51.6	74.7	34.3	28.6	27.8	51.6	65.6	
Ga	16.4	16.7	16.3	16.9	19.8	16.8	15.2	15.6	16.3	21.1	
Rb	89.9	128	215	70.3	119	159	178	157	100	80.4	
Sr	338	449	393	357	532	251	378	378	486	1136	
Y	23.10	20.74	7.29	15.81	22.53	27.13	16.39	16.43	12.90	9.88	
Zr	129	165	104	82	168	123	106	99	65	124	
Nb	5.80	8.19	7.40	6.88	9.55	12.7	10.4	11.1	5.04	8.81	
Cs	6.45	5.46	17.2	4.09	13.7	6.15	11.5	8.33	5.15	2.71	
Ba	617	603	736	311	330	530	839	638	631	1073	
La	19.1	29.4	20.8	13.6	31.0	36.1	42.3	45.6	37.4	44.8	
Ce	39.7	62.6	37.0	27.2	61.7	71.5	76.7	82.7	66.9	82.4	
Pr	4.76	7.36	3.88	3.23	7.29	8.20	8.00	8.50	6.82	9.01	
Nd	18.9	28.2	13.2	12.4	27.9	29.9	27.1	28.4	23.0	32.4	
Sm	4.17	5.39	2.11	2.68	5.36	5.84	4.60	4.75	3.50	5.03	
Eu	0.95	1.13	0.56	0.62	1.07	0.99	0.92	0.92	0.73	1.29	
Gd	4.05	4.63	1.63	2.51	4.58	4.71	3.36	3.40	2.82	3.48	
Tb	0.67	0.65	0.22	0.39	0.66	0.75	0.50	0.50	0.39	0.41	
Dy	3.93	3.67	1.25	2.46	3.88	4.42	2.75	2.66	2.18	1.94	
Ho	0.78	0.69	0.24	0.49	0.76	0.89	0.54	0.54	0.44	0.32	
Er	2.30	2.03	0.70	1.53	2.15	2.65	1.52	1.62	1.20	0.88	
Tm	0.35	0.31	0.10	0.24	0.34	0.39	0.24	0.25	0.17	0.12	
Yb	2.31	2.07	0.73	1.81	2.31	2.77	1.72	1.73	1.23	0.79	
Lu	0.37	0.32	0.12	0.30	0.38	0.40	0.26	0.29	0.19	0.12	
Hf	3.98	4.86	3.26	2.72	4.68	3.78	3.06	2.89	1.94	3.28	
Ta	0.50	0.69	0.74	0.89	0.79	1.38	0.94	1.01	0.43	0.51	

(continued on next page)

**Table 2** (continued)

Sample	06FW101	06FW104	06FW105	06FW108	06FW110	06FW111	06FW112	06FW118	06FW119	06FW120	06FW121
Age(Ma)	64.7	64.4	55.2	56.8	54.3	50.6	53.4	51.0	51.2	50.3	51.1
Pb	15.6	17.2	41.0	20.9	23.6	12.8	18.7	17.0	25.7	41.2	
Th	9.47	22.6	11.7	4.45	21.1	26.2	27.2	28.4	13.1	25.2	
U	1.21	5.82	3.28	1.52	4.47	4.61	5.84	5.11	2.01	3.29	
$\delta\text{Eu}$	0.70	0.68	0.88	0.72	0.65	0.56	0.68	0.66	0.69	0.89	
Sr/Y	14.6	21.7	53.8	22.6	23.6	9.2	23.0	23.0	37.6	114.9	
La/Yb	8.3	14.2	28.3	7.6	13.4	13.1	24.6	26.3	30.4	56.7	
$(\text{La}/\text{Yb})_{\text{N}}$	5.6	9.6	19.1	5.1	9.1	8.8	16.6	17.7	20.5	38.3	
$(\text{Yb})_{\text{N}}$	11.0	9.9	3.5	8.6	11.1	13.2	8.2	8.3	5.9	3.8	

TFe<sub>2</sub>O<sub>3</sub>: total Fe given as Fe<sub>2</sub>O<sub>3</sub>, A/CNK: molar Al<sub>2</sub>O<sub>3</sub>/(CaO + Na<sub>2</sub>O + K<sub>2</sub>O), Mg# = 100\*[Mg/(Mg + Fe)].

support their magmatic origin (Hoskin and Schaltegger, 2003), and their U-Pb ages represent the crystallization ages of the host granites.

Zircons in one granodiorite sample (08FW51) that was collected from southeast of Lhasa (Fig. 1b) yield a zircon  $^{206}\text{Pb}/^{238}\text{U}$  age of  $64.5 \pm 2.3$  Ma (Fig. 2a). The dating result resembles those of the two monzogranite samples from the Lhasa pluton with ages of  $64.7 \pm 1.1$  and  $64.4 \pm 0.9$  Ma (Ji et al., 2009a). Wen et al. (2008a) reported two coeval ages from Qulong ( $64.6 \pm 2.5$  Ma for a granite and  $64.0 \pm 1.4$  Ma for a diorite) and a relative young age of granite from easternmost of the Lhasa pluton ( $59.3 \pm 1.8$  Ma).

Four samples from northeast of Sangri have been dated (Fig. 1b). A granodiorite (SR03-1) gives the oldest age of  $59.8 \pm 0.9$  Ma, which is identical to the ages of a granite from the adjacent area ( $60.5 \pm 1.8$  Ma) and a granodiorite from Tsedong ( $60.1 \pm 1.4$  Ma) (Wen et al., 2008a). All other three samples (SR01-1, SR02-1 and SR04-1) have Eocene ages of  $45.4 \pm 0.7$  Ma,  $37.7 \pm 0.7$  Ma and  $42.1 \pm 0.7$  Ma, respectively; slightly younger than the Eocene granitoids identified in this region ( $48.9$ – $42.5$  Ma; Harrison et al., 2000) but older than the Yaja granodiorites (ca. 30 Ma) from east of Tsedong (Chung et al., 2009; Harrison et al., 2000).

Previous studies have paid little attention to the granitic rocks widespread in the northern Gyaca. We have traversed the Gangdese batholith from Gyaca to Cuijiu (Fig. 1b) and obtained four samples with ages ranging from late Paleocene to middle Eocene. Zircons from the southernmost granodiorite (09FW50) give a  $^{206}\text{Pb}/^{238}\text{U}$  age of  $50.2 \pm 1.9$  Ma, whereas the other three monzogranites (09FW41, 09FW42 and 09FW43), which locate at the northern part of the traverse have variable ages of  $56.1 \pm 1.1$  Ma (09FW41),  $50.7 \pm 1.1$  Ma (09FW42), and  $42.0 \pm 0.7$  Ma, respectively (Fig. 2f-i).

Abundant studies have focused on granitoids in the Nang-Mainling region, all of which are Cretaceous in age (108–68 Ma) (Guan et al., 2010; Quideleur et al., 1997; Wen et al., 2008a, 2008b; Zhang et al., 2010a; Zhu et al., 2011). In this study, we obtain an Eocene age in one granodiorite collected near Wolong between Nang and Mainling (Fig. 1b). Twenty-three analyzed spots give a mean  $^{206}\text{Pb}/^{238}\text{U}$  age of  $34.9 \pm 0.4$  Ma (Fig. 2j). To our knowledge, this is the first Eocene age reported in granitoids from this region and also the youngest Eocene magmatic age identified for the Gangdese batholith to date.

### 3.2. Major and trace elements

Samples from the Lhasa–Dazhuqu segment vary from gabbros to granites with ~52–77 wt.% SiO<sub>2</sub>. Samples from the Lhasa–Mainling segment consist mainly of granodiorites, monzogranites and granites with relatively restricted SiO<sub>2</sub> contents (~62–72 wt.%). All Gangdese samples belong to medium- to high-K calc-alkaline series, except one monzonite (sample 06FW139) that is shoshonitic

ic (Fig. 3a). This sample was dated at  $41.5 \pm 0.7$  Ma (Ji et al., 2009a). Most Gangdese samples are metaluminous and a few of them are weakly peraluminous (A/CNK = 0.74–1.08, Table 2) (Fig. 3b). All of them contain biotite and/or hornblende, and thus belong to I-type granitic rocks (Chappell and White, 1974).

Most samples show coherent trace element patterns (Fig. 4a–c), except two samples (06FW121 and 06FW127) with very high SiO<sub>2</sub> contents have very low contents of rare earth elements (REEs). As shown in Fig. 4d–f, most samples are enriched in large ion lithophile elements (LILE, e.g., Rb, Th, U and K), and light rare earth elements (LREE, e.g., La and Ce), and depleted in high field strength elements (HFSE, e.g., Nb, Ta and Ti) and heavy rare earth elements (HREE, e.g., Y and Lu). Furthermore, the samples display progressive changes along with ages, such as the element concentrations and fractionation of REE. For example, the enrichment in both Th and Pb becomes stronger from Paleocene to Middle-Late Eocene (Fig. 4d–f). All the Paleocene granitic rocks (65–56 Ma) show slightly fractionated REE patterns (Fig. 4a), with  $(\text{La}/\text{Yb})_{\text{N}}$  ratios of 8–17 and  $\text{Yb}_{\text{N}}$  of 7.6–17.4 (N: Chondrite normalized). The Early Eocene (56–48 Ma, Fig. 4b) and Middle-Late Eocene (48–34 Ma, Fig. 4c) samples have La/Yb ratio of 6–43 ( $\text{Yb}_{\text{N}} = 1.3$ –17.9) and La/Yb ratio of 13–161 ( $\text{Yb}_{\text{N}} = 3.2$ –11.1), respectively (Table 2). The evolution of REE for different period is evident when comparing its REE pattern with that of Oligo-Miocene adakites (Chung et al., 2003) (Fig. 4).

Some Early Eocene samples (50.2–51.2 Ma; 06FW119, 06FW147, 06FW148 and 09FW50) and most Middle-Late Eocene samples are characterized by high Sr contents (378–1136 ppm), low Y (7.01–18.78 ppm) and Yb (0.64–1.73 ppm) contents, and high Sr/Y (23–115). They also have high La/Yb (10–161) and display weak Eu anomaly ( $\delta\text{Eu} = 0.64$ –0.93, Table 2). These geochemical characteristics are similar to the Oligo-Miocene adakites noted above and are plotted into adakite and/or TTG fields (Fig. 5a and b).

### 3.3. Zircon Hf isotopes

Zircon Hf isotopes have been analyzed to constrain the isotope features of the source of the Gangdese granites in the southern Lhasa terrane. The  $\varepsilon_{\text{Hf}}(t)$  value is defined as the parts in  $10^4$  deviation of initial  $^{176}\text{Hf}/^{177}\text{Hf}$  isotopic ratios between the sample and the chondritic uniform reservoir (CHUR), and it is calculated after Griffin et al. (2002). The  $\varepsilon_{\text{Hf}}(t)$  vs. zircon U–Pb age diagram shows the evolution of Hf isotopes along with time (Fig. 6).

Zircons in sample 08FW51 from southeastern Lhasa have  $^{176}\text{Hf}/^{177}\text{Hf}$  ranging from 0.282998 to 0.283069 and  $\varepsilon_{\text{Hf}}(t)$  values of 9.52–11.97 (mean =  $10.7 \pm 0.4$ ; n = 16), which are higher than those of the Lhasa pluton ( $7.9 \pm 0.3$  and  $6.0 \pm 0.4$ ) (Ji et al., 2009a).

Zircons from the Paleocene Sangri granodiorite SR03-1 ( $59.8 \pm 0.9$  Ma) have  $^{176}\text{Hf}/^{177}\text{Hf}$  ratios of 0.282903–0.283036, giving a weighted  $\varepsilon_{\text{Hf}}(t)$  value of  $7.9 \pm 0.5$ . Three Eocene samples (SR01-1, SR02-1 and SR04-1) show  $\varepsilon_{\text{Hf}}(t)$  values ranging from

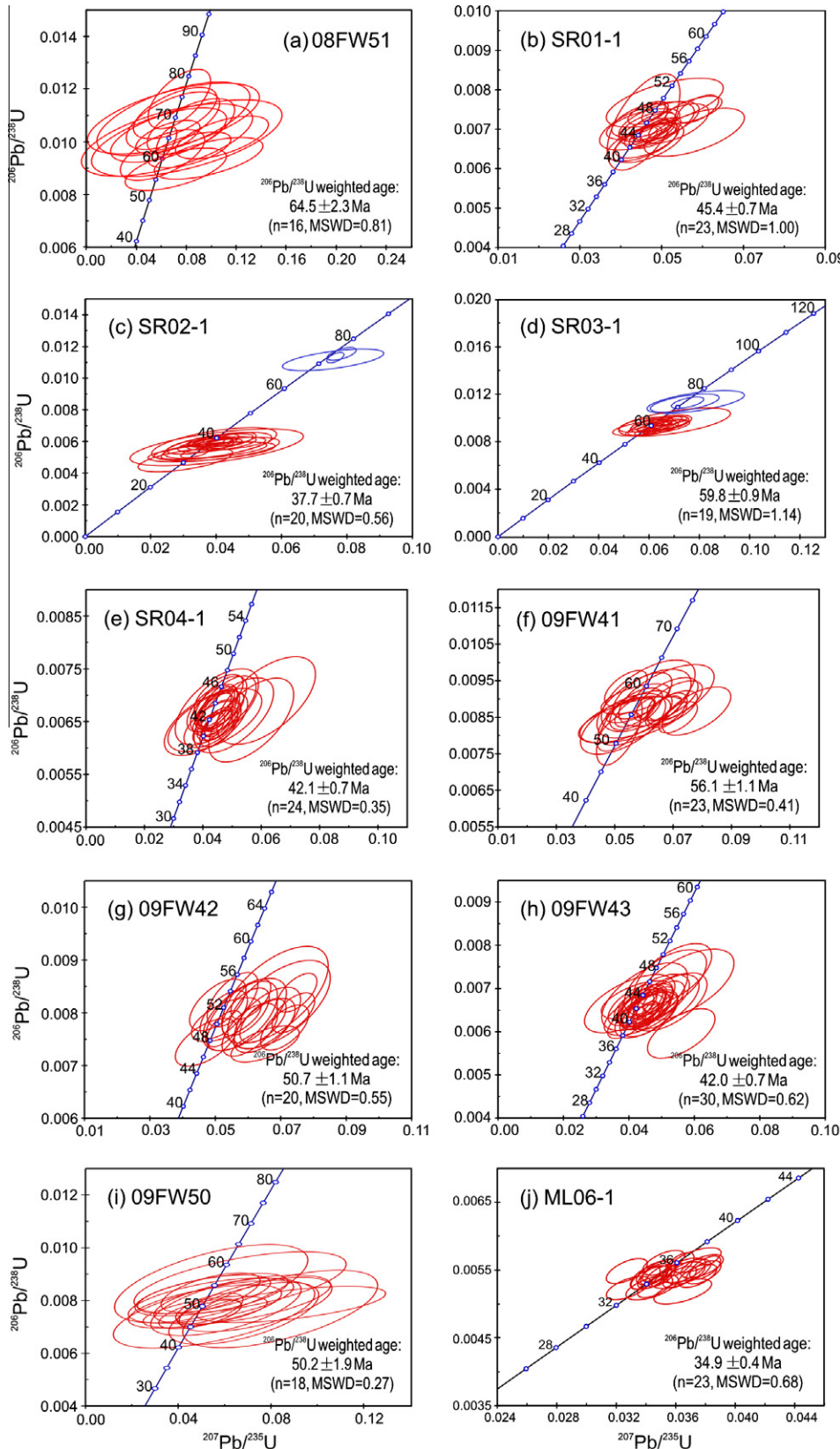
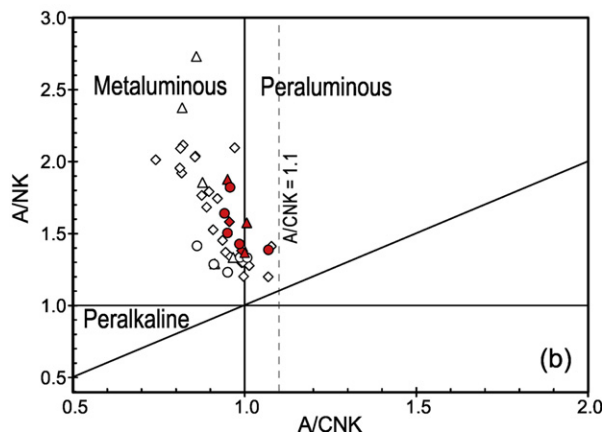
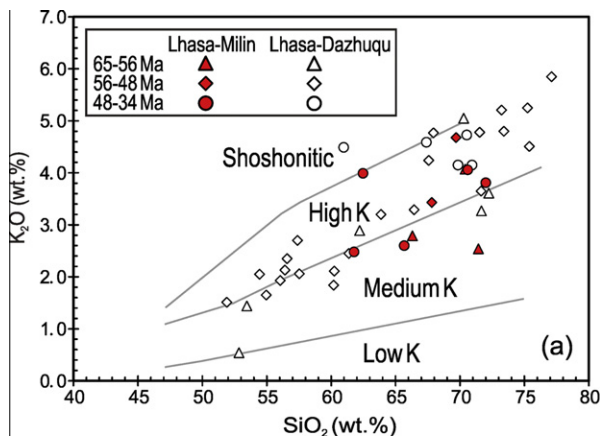


Fig. 2. Zircon U-Pb concordia diagrams of granites from Lhasa-Mainling segment.

$6.2 \pm 0.8$  to  $9.2 \pm 0.4$  (Table 1). It is evident that the  $\varepsilon_{\text{Hf}}(t)$  values become smaller with the decrease in age. Because these samples were collected from the same region, such a trend should reflect

the change in the source materials, i.e., more ancient materials were involved along with the partial melting. Such a trend was at least lasted until early Oligocene, as supported by the lower



**Fig. 3.** (a)  $SiO_2$  vs.  $K_2O$  diagram and (b)  $A/CNK$  vs.  $A/NK$  diagram for rocks from the Gangdese batholith.

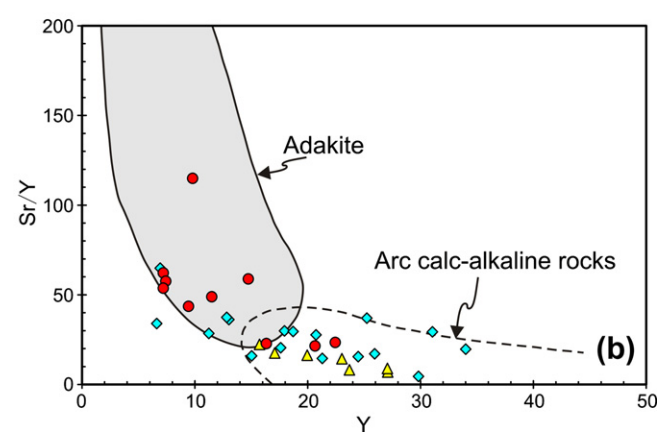
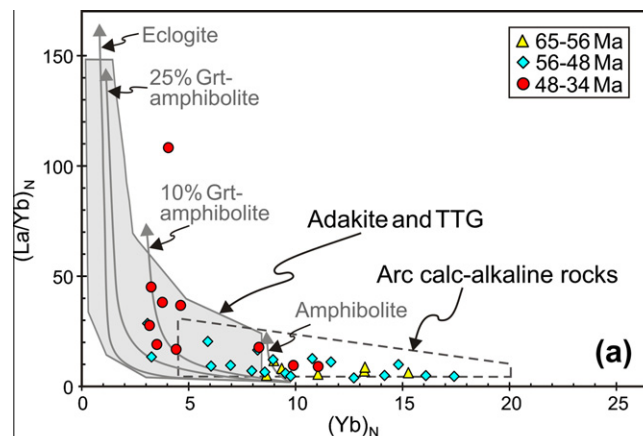


**Fig. 5.** Plots of (a)  $(La/Yb)_N$  vs.  $(Yb)_N$  and (b)  $Sr/Y$  vs.  $Y$  for a subset of samples in this study with  $>56$  wt.%  $SiO_2$ . The subscript N denotes chondrite-normalized values.

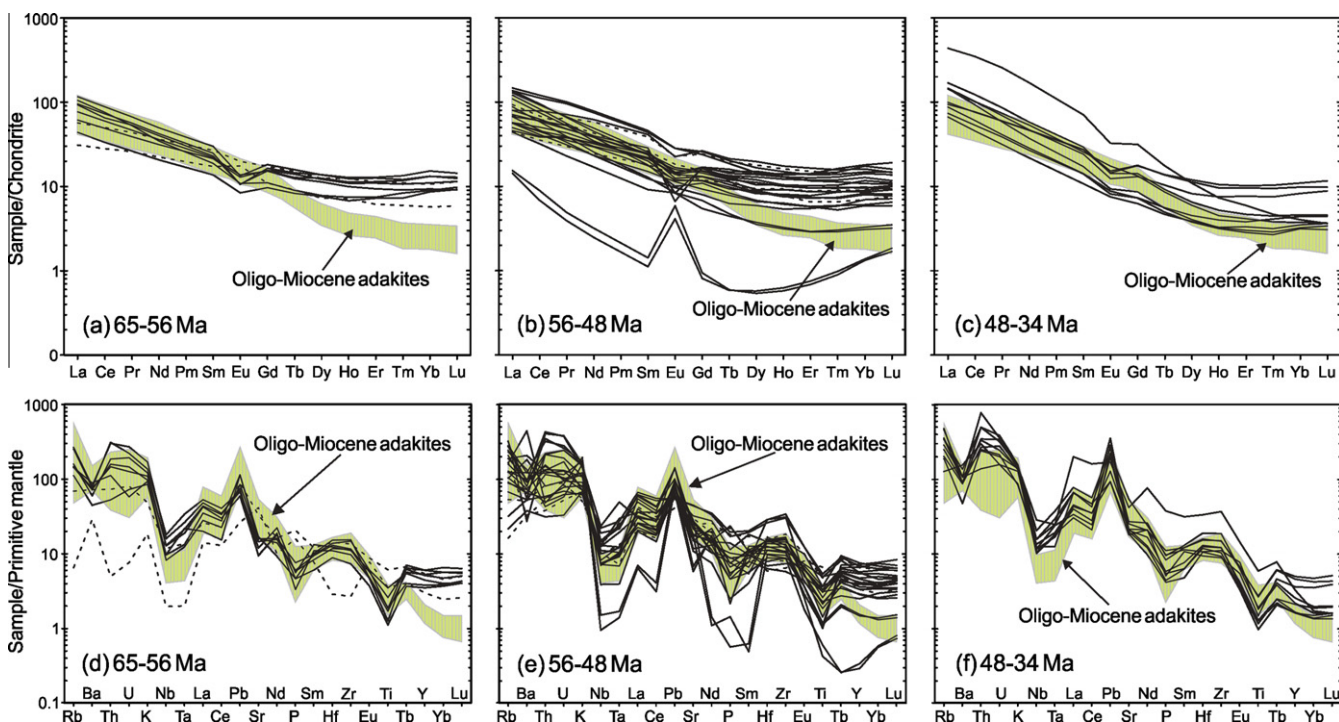


**Fig. 4.** Chondrite-normalized REE variation diagram and primitive mantle-normalized spiderdiagram for rocks from the Gangdese batholith. Dashed lines denote samples with  $<56$  wt.%  $SiO_2$ .

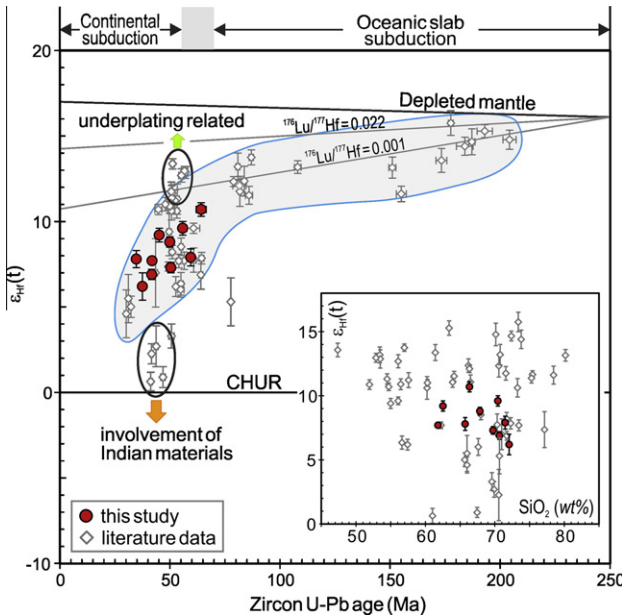


**Fig. 6.** Binary plot of  $\varepsilon_{\text{Hf}}(t)$  values vs. U-Pb ages of Gangdese batholith. Inset shows the variations between  $\varepsilon_{\text{Hf}}(t)$  values and  $\text{SiO}_2$  contents. Data after Chu et al. (2006), Chung et al. (2009), Guan et al. (2010), Huang et al. (2010), Ji et al. (2009a), Zhang et al. (2007), Zhu et al. (2011), and this study.

$\varepsilon_{\text{Hf}}(t)$  values ( $5.1 \pm 0.9$ ) reported in a Yaja granodiorite with an age of ca. 30 Ma (Chung et al., 2009).

Zircons in sample 09FW50 from the north of Gyaca show a limited variation in  $^{176}\text{Hf}/^{177}\text{Hf}$  (0.282963–0.283014) and  $\varepsilon_{\text{Hf}}(t)$  values of 7.84–9.62. Three monzogranites from the south of Cuijiu have  $\varepsilon_{\text{Hf}}(t)$  values ranging from  $9.6 \pm 0.4$  to  $6.9 \pm 0.3$  and display a trend similar to Sangri Eocene granitic rocks, reflecting the increasing contributions of old materials from 56 Ma to 42 Ma.

Zircons from the Wolong granodiorite ( $34.9 \pm 0.4$  Ma) have variable  $^{176}\text{Hf}/^{177}\text{Hf}$  of 0.282892–0.283034 and  $\varepsilon_{\text{Hf}}(t)$  values of 4.99–10.01. A remarkably high  $^{176}\text{Hf}/^{177}\text{Hf}$  of 0.283068 and  $\varepsilon_{\text{Hf}}(t)$  value of 11.86 was obtained from an inherited zircon with an age of 65 Ma (Table A2).

#### 4. Discussion

##### 4.1. Trace element constraint for crustal thickening

Samples from the Gangdese batholith show similar trace element patterns and systematic variations in compositions with time (Fig. 4). For example, concentrations of light rare earth elements (LREEs) and large ion lithophile elements (LILEs) increase from 65–56 Ma through 56–48 Ma to 48–34 Ma (Table 2). Furthermore, the Paleocene samples have high heavy rare earth elements (HREE) contents (e.g. 1.20–3.19 ppm Yb) (Fig. 4a), whereas part of the Early Eocene (Fig. 4b) and most of the Middle–Late Eocene (Fig. 4c) samples have low contents of HREE (0.64–1.79 ppm Yb) and strongly-fractionated REE patterns ( $\text{La/Yb} = 10$ –161). These variations are probably related to crustal thickening processes (McMillan et al., 1993). Some Eocene samples show geochemical characteristics similar to the Oligo–Miocene adakites (Fig. 4b and c), which crop out in the southern Lhasa terrane (Chung et al., 2003, 2009). Adakites are characterized by elevated Sr/Y and La/Yb features, commonly ascribed to partial melting of garnet-bearing amphibolite or eclogite at P-T conditions under which garnet and/or amphibolite is stable but plagioclase is unstable (Martin, 1999 and references therein). Therefore, these trace element ratios

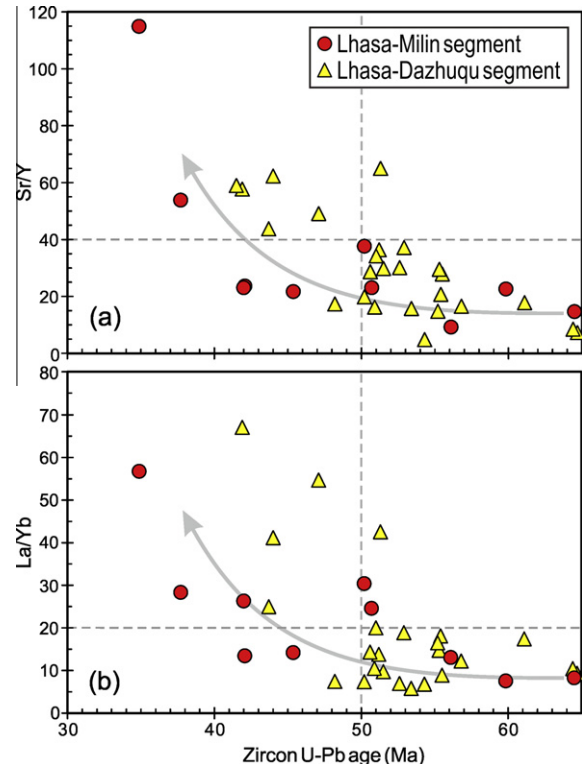


**Fig. 7.** Plots of (a) Sr/Y and (b) La/Yb ratios vs. magmatic ages for a subset of samples in this study with 56–75 wt.%  $\text{SiO}_2$ .

have been widely applied to discriminate adakitic rocks from typical arc-related calc-alkaline rocks (Defant and Drummond, 1990; Martin, 1986). Also, the ratios are used as indicators of the crustal thickness (Chung et al., 2009; Haschke et al., 2002; Martin, 1986). The systematic variations of Sr/Y and La/Yb ratios reflect the variable contents of residual garnet and amphibole.

Our samples show marked increases in La/Yb and Sr/Y from Paleocene to Late Eocene (Fig. 7). This indicates the crust in both Lhasa–Mainling and Lhasa–Dazhuqu segments was continuously thickened during this period. All the Paleocene rocks with low Sr/Y (<40) and La/Yb (<20) ratios (Fig. 7) were derived from normal and unthickened crust, i.e., ca. 35 km. Both Sr/Y and La/Yb ratios were increased since the late Early Eocene. Most Middle–Late Eocene granitoids have Sr/Y (>40) and La/Yb (>20) similar to those of adakitic rocks. The crustal thickening processes are better demonstrated in localities with continuous magmatic records, such as east of Quxu, northeast of Sangri, and south of Cuijiu (Table 2). For instance, granitic rocks were emplaced from 47.1 to 41.5 Ma in east of Quxu (06FW131–139; Ji et al., 2009a); their Sr/Y and La/Yb increase from 49 to 59 and from 55 to 161, respectively. The Paleocene Sangri granodiorite (59.8 Ma) has Sr/Y of 23 and La/Yb of 8, whereas the Early Middle–Eocene granodiorites (45.4–42.1 Ma) have Sr/Y and La/Yb of 22–24 and 13–14, respectively. However, the Sr/Y and La/Yb increase to 54 and 28, respectively, in the Late Middle–Eocene granite (37.7 Ma).

It has been suggested that the REE patterns can be fractionated by retention of amphibole in the source region or low-pressure fractionation of amphibole. Without involvement of garnet, however, amphibole alone would result in concave upward REE patterns with depletions in MREE and increase the La/Yb as high as 14–15 (Kay et al., 1989). Thus, high La/Yb and fractionated REE patterns shown by the Gangdese granitoids require a garnet amphibolite source (Fig. 5a). Garnet can be stable in mafic sources at crustal thickness greater than 40 km i.e.,  $\geq 1.2$  GPa (Rapp and

Watson, 1995). Therefore, the Gangdese granitoids support that the crust beneath the southern Lhasa terrane was locally thickened to >40 km by ~51 Ma. The Late Eocene granitoids, including samples from east of Quxu (06FW134 and 06FW139) and Wolong (ML06-1), have La/Yb larger than 55, indicating crustal thickness of 50–55 km (Chung et al., 2009; Haschke et al., 2002).

#### 4.2. Zircon Hf isotope variation along with crustal thickening

The Lu-Hf isotope system is an important geochemical tracer for deciphering petrogenesis and crustal evolution (Griffin et al., 2002; Kinny and Maas, 2003). Zircon Hf isotopes of granitic rocks from the Lhasa terrane have been widely reported in recent literatures (Chiu et al., 2009; Chu et al., 2006; Chung et al., 2009; Ji et al., 2009a; Ji, 2010; Liang et al., 2008; Zhang et al., 2007, 2010b; Zhu et al., 2009a,b,c; Zhu et al., 2011). The results show that the Mesozoic granitoids of Gangdese batholith from the southern Lhasa terrane have highly radiogenic Hf isotopes, with  $\varepsilon_{\text{Hf}}(t)$  values commonly larger than 11 (Fig. 6). The evolutionary trajectory shown by these data intersects the depleted mantle array in late Paleozoic or early Mesozoic (cf. Fig. 10, Ji et al., 2009a), which reflects significant addition of juvenile mantle materials at that time. These author also noted that both crust and mantle of the southern Lhasa terrane show similar primitive Hf isotopic compositions. As shown in Fig. 6, the Hf isotopes do not show any correlation with SiO<sub>2</sub>. This suggests that the primitive isotopic compositions were not obviously affected by either involvement of crustal rocks in the source or during magmatic evolution. This is supported by the fact that very few Precambrian zircons were identified from Gangdese batholith (cf. Ji et al., 2009a; Wen et al., 2008a). Therefore, a little ancient basement existed in the southern Lhasa terrane, which is perhaps locally distributed or only survived at very shallow depth.

Most of the Cenozoic samples show a clear decreasing tendency of Hf isotopes (Fig. 6), which cannot be directly evolved from the Mesozoic granitoids but requires the involvement of ancient and enriched materials. As discussed above, the ancient components did not exist in the southern Lhasa terrane during the Mesozoic. Therefore, such ancient materials are exotic and start to be involved into the deep petrogenetic process since Early Cenozoic. Along with the decreasing ages, the  $\varepsilon_{\text{Hf}}(t)$  values decrease (Fig. 6) and the La/Yb and Sr/Y ratios increase (Fig. 7). This implies a relation between the crustal thickening and the addition of ancient materials.

#### 4.3. Possible mechanisms for crustal thickening

The initial age of the India–Asia collision provides an important constraint on the mechanism of crustal thickening. It becomes a consensus that the India–Asia continental collision resulted in the crustal thickening of the Tibetan plateau, as the thickened crust has been recognized by geophysical observations (Zhao et al., 2004 and references therein). Currently, it is highly debated on the initial collision age, from ~70 to ~34 Ma (cf. Aitchison et al., 2007; Yin and Harrison, 2000). However, most of the arguments focused at 55 ± 5 Ma (see Wu et al., 2008 for a review). Therefore, the crustal thickening identified in this study commenced after the initial continental collision.

Traditionally, both magma underplating (Gill, 1981) and/or crustal shortening (Sheffels, 1990) have been proposed for crustal thickening at subduction zones. Crustal thickening in the Tibetan plateau has been previously ascribed to tectonic processes, such as lithosphere shortening, crustal injection, and underthrusting (as discussed above). The role of magmatism played in crustal thickening was emphasized in recent studies (Chung et al., 2009; Mo et al., 2007). Highly radiogenic Hf isotopes of Mesozoic grani-

toids from the Gangdese batholith support the existence of juvenile basement (Fig. 6), and melting of the juvenile crust would give rise to the Cenozoic granitoids with primitive Hf isotopes. Therefore, it should be careful to discriminate the addition of juvenile materials from the mantle and the recycling of juvenile crust.

##### 4.3.1. Basaltic underplating

Underplating of basaltic magmas was invoked to account for crustal thickening in the Andes (Atherton and Petford, 1993; Haschke et al., 2002). Extensive basaltic magmatism can be produced not only through partial melting of the mantle wedge induced by slab-derived fluids/melts but also by decompressional melting of asthenospheric mantle in extensional settings (Furlong and Fountain, 1986), such as lithosphere extension (McKenzie, 1978) and delamination (Bird, 1979). Widespread basaltic magmatism is a precondition of basaltic underplating. However, subduction of cold, dry and refractory continental lithosphere is unlikely to produce massive basaltic magmas.

The following evidences support that basaltic underplating could have occurred from Late Cretaceous to Early Eocene. Several studies have shown that the Lhasa terrane underwent strong crustal shortening and thickening during the Cretaceous (Kapp et al., 2007; Murphy et al., 1997), which is also supported by the late Cretaceous (ca. 90–78 Ma) adakitic rocks (Guan et al., 2010; Meng et al., 2010; Wen et al., 2008b; Zhang et al., 2010a). The lower portion of the thickened lithospheric mantle was delaminated at ca. 69 Ma (Kapp et al., 2007). Compositions of the Paleocene granitoids indicate that they were derived from crust of normal thickness (ca. 35 km), which also supports the removal of thickened root in the Lhasa terrane before the Cenozoic. The lithosphere delamination would result in the upwelling of hot asthenosphere and its decompressional melting thus lead to the massive basaltic underplating in the mantle wedge. The delaminated mantle accelerated the rollback of the subducted Tethyan slab and ultimately led to its break-off at ca. 50 Ma (Chung et al., 2005; Lee et al., 2009), which also led to large-scale magma underplating. As presented in Table 2, some low-SiO<sub>2</sub> rocks (52–56 wt.%) emplaced during 57–50 Ma show remarkably primitive Hf isotopic compositions, which are distinct from the decreasing trend of the Cenozoic granitoids (Fig. 6). This indicates that these rocks originated from the asthenosphere or depleted lithosphere mantle. Based on study of mafic rocks from the Gangdese batholith, Dong et al. (2005) suggested the possibility of magma underplating of 53–47 Ma which resulted in the widespread mafic rocks in the southern margin of the Lhasa terrane. These lines of evidence imply that widely magma underplating should have happened from Late Cretaceous to Early Eocene time.

Some adakitic granitoids are spatially associated with the mafic rocks during the magmatic peak, which can be generated by different processes, e.g., partial melting of the subducted oceanic slab (Defant and Drummond, 1990), fractional crystallization of coeval mafic rocks (Macpherson et al., 2006), partial melting of newly underplated basaltic crust (Atherton and Petford, 1993), thickened (Chung et al., 2003) or delaminated (Xu et al., 2002; Gao et al., 2004) lower crust. Adakites have been originally explained by partial melting of the subducted young (<25 Ma) and hot oceanic crust (Defant and Drummond, 1990). However, the old subducted slab can be melted when enough heat is provided. For example, adakites was also explained by the slab tears model, in which the edge of the subducting plate is heated by mantle flow (Yogodzinski et al., 2001). In this scenario, the adakitic melts would interact with mantle peridotite and have high Mg# values (Rapp et al., 1999). However, low Mg# values (39–46) of the adakitic granitoids in the Lhasa terrane do not favor this model. It has been suggested that geochemical features of adakites can be achieved through fractional crystallization of mafic rocks (Macpherson et al., 2006). Four samples from Niedang with compositions from diorite to

granite, in which one adakitic granodiorite (06FW118) is included, have been used to study the effects of fractional crystallization. Their trace elements do not follow the trend of fractional crystallization, for which the La/Sr should keep constant with the increase of La contents (Table 2). Low Mg# values and the widely magma underplating during Paleocene and Early Eocene in the southern Lhasa terrane suggest that the adakitic granitoids with ages of ca. 51 Ma were probably derived from partial melting of the newly underplated basaltic crust, similar to the sodium-rich, adakitic granites from the Cordillera Blanca complex in the Andes (Atherton and Petford, 1993). Thus, massive basaltic underplating in the early Cenozoic resulted in the early crustal thickening of the southern Lhasa terrane, and adakitic granitoids of ~51 Ma are derived from the newly underplated basaltic crust.

#### 4.3.2. Addition of Indian materials

Many of the Middle–Late Eocene granitoids (47–34 Ma) in the Lhasa terrane are potassium-rich (Table 2) and different from the adakites produced by melting of newly underplated basaltic crust (Atherton and Petford, 1993). Furthermore, subduction of the Indian continental lithosphere after continental collision is difficult to result in massive partial melting of the mantle wedge and asthenosphere. Therefore, some other mechanisms are required to explain the long-lasting crustal thickening (50–34 Ma) in the Lhasa terrane.

As presented in the Fig. 6, the zircon Hf isotopes start to decrease since the Early Cenozoic, which is coeval with or slightly earlier than the initial continental collision. Both Th and Pb contents gradually increase along with the decreasing Hf isotopic compositions (Fig. 4b). Low radiogenic Hf isotopes and high Th and Pb abundances are characteristics of mature continental crust. The Indian continent to the south (Zeng et al., 2011) and the central Lhasa terrane (Zhu et al., 2011) to the north are both composed of ancient materials, thus either or both of them could be the candidate. During the Mesozoic era, long-term magmatism developed in the southern Lhasa terrane, most of which exhibit very primitive isotopic composition (Fig. 6), without obvious contamination of ancient materials identified, which excluded the possible contribution from the central Lhasa terrane on the magma generation of the southern Lhasa terrane. Thus, we do not anticipate it play an important role in the Cenozoic magmatism of the southern Lhasa terrane. Following the northward movement of the Indian continent and its direct subduction, more ancient materials from the passive margin would be involved during the magma generation. Therefore, the Indian continent is a more likely candidate for the old components. For example, granitoids from Tethyan Himalaya exhibit low Nd isotopic compositions and high concentrations of Th and Pb (Xie et al., 2010). The Paleocene granitoids do not follow the crustal thickening trend (Fig. 7), but have  $^{176}\text{Hf}/^{177}\text{Hf}$  lower than the Mesozoic granitoids. This suggests that the old materials, e.g., sediments from passive continental margin, have obviously increased in Early Cenozoic following the convergence between India and Asia (Chu et al., 2011). Some samples with remarkably low and variable Hf isotopes (Fig. 6) reflect the involvement of abundant Indian materials during partial melting following the slab break-off.

#### 4.3.3. Indian indentation

As discussed above, the southern Lhasa terrane should have undergone widespread underplating from Late Cretaceous to Early Eocene during the geological process including delamination, slab roll-back and break-off. And the southern Lhasa terrane was underlain by a thermal and hydrous (due to the early oceanic subduction) lithosphere, which could be proved by the long lasting magmatic activity in the Eocene epoch. The long term thermal status would induce the weakening and softening of the lower crust and mantle wedge, thus facilitates the indentation of the hard In-

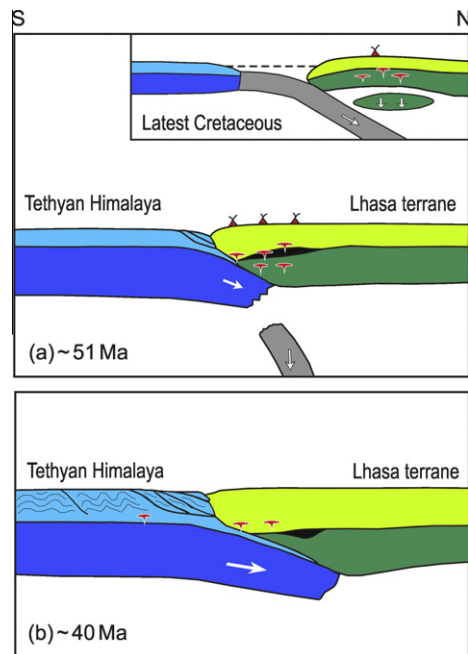


**Fig. 8.** Schematic diagrams illustrating Eocene crustal thickening in the southern Lhasa terrane, Tibet. The southern Lhasa terrane underwent continuous crustal thickening in Eocene, and (a) it already underlaid a thickened crust locally in early Eocene (~51 Ma) due to basaltic underplating, while (b) the latter stage is ascribed to addition of Indian materials and indentation of Indian continent.

dian continent and the homogeneous/distributed thickening of the southern Lhasa terrane (Chung et al., 2009). Chung et al. (2009) emphasized that the precollisional geodynamic processes constrained the initial conditions and evolution of the orogenesis, and the tectonic thickening induced by Indian indentation is easy for the thermally softened lithosphere of the southern Lhasa terrane. The thermally softened status also insulates the deformation and constrains that in the depth, which can explain why no obvious compressional deformation developed on the surface of the Lhasa terrane in Early Tertiary.

In a word, the protracted thermal status in the deep crust precludes the possibility of large-scale injection of Indian crust. And the progressive crustal thickening during this period does not favor the underthrusting model. Therefore, we suggest that basaltic underplating (>ca. 51 Ma), involvement of Indian materials and Indian indentation account for the crustal thickening of the Lhasa terrane in the Eocene (Fig. 8).

## 5. Concluding remarks

- (1) The Transhimalayan magmatism was continuous from Paleocene to Eocene (ca. 65–34 Ma) and resulted in the emplacement of the Gangdese batholith.
- (2) The southern Lhasa terrane has a prolonged history of crustal thickening in the Eocene and a thickened crust existed, at least locally, since ca. 51 Ma.
- (3) The Eocene crustal thickening in the Lhasa terrane resulted from a variety of magmatic and tectonic processes, including basaltic underplating, addition of Indian materials and shortening caused by the Indian indentation.

## Acknowledgements

We are grateful to the constructive reviews from Prof. Ji-Feng Xu and Prof. Di-Cheng Zhu, and the English polishing by Dr.

Kwan-Nang Pang. We thank staffs of MC-ICPMS and XRF laboratories at the Chinese Academy of Sciences for help with zircon and major element analyses, respectively; staffs of LA-ICPMS laboratory at State Key Laboratory of Geological Processed and Mineral Resources, the China University of Geosciences, Wuhan, for help with trace element analyses. This study was supported by research grants from the Chinese Academy of Sciences (KZCX2-YW-Q09-06) and the National Natural Science Foundation of China (No. 40721062).

## Appendix A. Supplementary data

Supplementary data associated with this article can be found, in the online version, at doi:10.1016/j.jseas.2011.08.020.

## References

- Aitchison, J.C., Ali, J.R., Davis, A.M., 2007. When and where did India and Asia collide? *Journal of Geophysical Research* 112, B05423. doi:10.1029/2006JB004706.
- Argand, E., 1924. La tectonique de l'Asie. *International Geological Congress Report Session 13* (1), 170–372.
- Atherton, M.P., Petford, N., 1993. Generation of sodium-rich magmas from newly underplated basaltic crust. *Nature* 362, 144–146.
- Bird, P., 1979. Continental delamination and the Colorado Plateau. *Journal of Geophysical Research* 84, 7561–7571.
- Chappell, B.W., White, A.J.R., 1974. Two contrasting granite types. *Pacific Geology* 8, 173–174.
- Chiu, H.Y., Chung, S.-L., Wu, F.-Y., Liu, D., Liang, Y.-H., Lin, I.-J., Iizuka, Y., Xie, L.-W., Wang, Y., Chu, M.-F., 2009. Zircon U–Pb and Hf isotopic constraints from eastern Transhimalayan batholiths on the precollisional magmatic and tectonic evolution in southern Tibet. *Tectonophysics* 477, 3–19.
- Chu, M.F., Chung, S.L., Song, B., Liu, D.Y., O'Reilly, S.Y., Pearson, N.J., Ji, J.Q., Wen, D.J., 2006. Zircon U–Pb and Hf isotope constraints on the Mesozoic tectonics and crustal evolution of Southern Tibet. *Geology* 34, 745–748.
- Chu, M.F., Chung, S.L., O'Reilly, S.Y., Pearson, N.J., Wu, F.Y., Li, X.H., Liu, D.Y., Ji, J.Q., Chu, C.H., Lee, H.Y., 2011. India's hidden inputs to Tibetan orogeny revealed by Hf isotopes of Transhimalayan zircons and host rocks. *Earth and Planetary Science Letters* 307, 479–486.
- Chung, S.L., Chu, M.F., Ji, J.Q., O'Reilly, S.Y., Pearson, N.J., Liu, D.Y., Lee, T.Y., Lo, C.H., 2009. The nature and timing of crustal thickening in Southern Tibet: geochemical and zircon Hf isotopic constraints from postcollisional adakites. *Tectonophysics* 477, 36–48.
- Chung, S.L., Chu, M.F., Zhang, Y.Q., Xie, Y.W., Lo, C.H., Lee, T.Y., Lan, C.Y., Li, X.H., Zhang, Q., Wang, Y.Z., 2005. Tibetan tectonic evolution inferred from spatial and temporal variations in post-collisional magmatism. *Earth-Science Reviews* 68, 173–196.
- Chung, S.L., Liu, D.Y., Ji, J.Q., Chu, M.F., Lee, H.Y., Wen, D.J., Lo, C.H., Lee, T.Y., Qian, Q., Zhang, Q., 2003. Adakites from continental collision zones: melting of thickened lower crust beneath southern Tibet. *Geology* 31, 1021–1024.
- Coulon, C., Maluski, H., Bollinger, C., Wang, S., 1986. Mesozoic and Cenozoic volcanic rocks from central and southern Tibet:  $^{39}\text{Ar}/^{40}\text{Ar}$  dating, petrological characteristics and geodynamical significance. *Earth and Planetary Science Letters* 79, 281–302.
- Debon, F., Le Fort, P., Sheppard, S.M., Sonet, J., 1986. The four plutonic belts of the Transhimalaya-Himalaya: a chemical, mineralogical, isotopic, and chronological synthesis along a Tibet-Nepal section. *Journal of Petrology* 27, 219–250.
- Defant, M.J., Drummond, M.S., 1990. Derivation of some modern arc magmas by melting of young subducted lithosphere. *Nature* 347, 662–666.
- Dewey, J.F., Shackleton, R.M., Chang, C., Sun, Y., 1988. The tectonic evolution of the Tibetan plateau. *Philosophical Transactions of the Royal Society, London A327*, 379–413.
- Dong, G.C., Mo, X.X., Zhao, Z.D., Guo, T.Y., Wang, L.L., Chen, T., 2005. Geochronologic constraints on the magmatic underplating of the Gangdese belt in the India-Eurasia collision: evidence of SHRIMP II zircon U-Pb dating. *Acta Geologica Sinica* 79, 787–794.
- Dürr, S.B., 1996. Provenance of Xigaze fore-arc basin clastic rocks (Cretaceous, south Tibet). *Geological Society of America Bulletin* 108, 669–684.
- Einsele, G., Liu, B., Durr, S., Frisch, W., Liu, G., Luterbacher, H.P., Ratschbacher, L., Ricken, W., Wendt, J., Wetzel, A., Yu, G., Zheng, H., 1994. The Xigaze forearc basin: Evolution and facies architecture (Cretaceous, Tibet). *Sedimentary Geology* 90, 1–32.
- England, P.C., Houseman, G.A., 1986. Finite strain calculations of continental deformation 2. Comparison with the India-Asia collision. *Journal of Geophysical Research* 91, 3664–3676.
- Furlong, K., Fountain, D.M., 1986. Continental crustal underplating: thermal considerations and seismic-petrological consequences. *Journal of Geophysical Research* 91, 8285–8294.
- Gao, S., Rudnick, R.L., Yuan, H.L., Liu, X.M., Liu, Y.S., Xu, W.L., Lin, W.L., Ayers, J., Wang, X.C., Wang, Q.H., 2004. Recycling lower continental crust in the North China craton. *Nature* 432, 892–897.
- Gill, J., 1981. *Orogenic Andesites and Plate Tectonics*. New York, Springer-Verlag, p. 390.
- Griffin, W.L., Wang, X., Jackson, S.E., Pearson, N.J., O'Reilly, S.Y., Xu, X.S., Zhou, X.M., 2002. Zircon chemistry and magma mixing, SE China: in-situ analysis of Hf isotopes, Tonglu and Pingtan igneous complexes. *Lithos* 2002, 237–269.
- Guan, Q., Zhu, D.C., Zhao, Z.D., Zhang, L.L., Liu, M., Li, X.W., Yu, F., Mo, X.X., 2010. Late Cretaceous adakites in the eastern segment of the Gangdese Belt, southern Tibet: Products of Neo-Tethyan ridge subduction? *Acta Petrologica Sinica* 26, 2165–2179.
- Guynn, J.H., Kapp, P., Pullen, A., Gehrels, G., Heizler, M., Ding, L., 2006. Tibetan basement rocks near Amdo reveal "missing" Mesozoic tectonism along the Bangong suture, central Tibet. *Geology* 34, 505–508.
- Harris, N.B.W., Xu, R., Lewis, C.L., Jin, C.W., 1988. Plutonic rocks of the 1985 Tibet Geotraverse, Lhasa to Golmud. *Philosophical Transactions of the Royal Society, London A327*, 145–168.
- Harrison, T.M., Yin, A., Grove, M., Lovera, O.M., Ryerson, F.J., Zhou, X., 2000. The Zedong Window: a record of superposed Tertiary convergence in southeastern Tibet. *Journal of Geophysical Research* 105, 19211–19230.
- Haschke, M., Siebel, W., Günther, A., Scheuber, E., 2002. Repeated crustal thickening and recycling during the Andean orogeny in north Chile (21–26 S). *Journal of Geophysical Research* 107. doi:10.1029/2001JB000328.
- He, S.D., Kapp, P., DeCelles, P.G., Gehrels, G.E., Heizler, M., 2007. Cretaceous-Tertiary geology of the Gangdese Arc in the Linzhou area, southern Tibet. *Tectonophysics* 443, 15–37.
- Hoskin, P.W.O., Schaltegger, U., 2003. The composition of zircon and igneous and metamorphic petrogenesis. In: Manchar, J.M., Hoskin, P.W.O. (Eds.), *Zircon. Reviews of Mineralogy and Geochemistry*, vol. 53, pp. 27–62.
- Hou, Z.Q., Gao, Y.F., Qu, X.M., Rui, Z.Y., Mo, X.X., 2004. Origin of adakitic intrusives generated during mid-Miocene east-west extension in southern Tibet. *Earth and Planetary Science Letters* 220, 139–155.
- Hu, D.G., Wu, Z.H., Jiang, W., Shi, Y.R., Ye, P.S., Liu, Q.S., 2005. SHRIMP zircon U-Pb age and Nd isotopic study on the Nyainqntanglha Group in Tibet. *Science in China (Series D)* 48, 1377–1386.
- Huang, Y., Zhao, Z.D., Zhang, F.Q., Zhu, D.C., Dong, G.C., Mo, X.X., 2010. Geochemistry and implication of the Gangdese batholiths from Renbu and Lhasa areas in southern Gangdese, Tibet. *Acta Petrologica Sinica* 26, 3131–3142.
- Ji, W.Q., Wu, F.Y., Chung, S.L., Li, J.X., Liu, C.Z., 2009a. Zircon U-Pb chronology and Hf isotopic constraints on the petrogenesis of Gangdese batholiths, southern Tibet. *Chemical Geology* 262, 229–245.
- Ji, W.Q., Wu, F.Y., Liu, C.Z., Chung, S.L., 2009b. Geochronology and petrogenesis of granitic rocks in Gangdese batholith, southern Tibet. *Science in China (Series D)* 52, 1240–1261.
- Ji, W.Q., 2010. Geochronology and petrogenesis of granitic rocks from east segment of the Gangdese batholith, southern Tibet. Unpublished result. PhD thesis, Chinese Academy of Sciences.
- Jackson, J.A., Austheim, H., McKenzie, D., Priestley, K., 2004. Metastability, mechanical strength, and the support of mountain belts. *Geology* 32, 625–628.
- Johnson, M.R.W., 2002. Shortening budgets and the role of continental subduction during the India-Asia collision. *Earth-Science Reviews* 59, 101–123.
- Kang, Z.Q., Xu, J.F., Dong, Y.H., Wang, B.D., 2008. Cretaceous volcanic rocks of Zenong Group in north-middle Lhasa block: products of southward subducting of the Slainajap Ocean? *Acta Petrologica Sinica* 24, 303–314 (in Chinese with English abstract).
- Kapp, P., Decelles, P.G., Leier, A.L., Fabijanic, J.M., He, S.D., Pullen, A., Gehrels, G.E., 2007. The Gangdese retroarc thrust belt revealed. *GSA Today* 17. doi:10.1130/GSAT01707A.1.
- Kay, S.M., Ramos, V.A., Mpodozis, C., Sruoga, P., 1989. Late Paleozoic to Jurassic silicic magmatism at the Gondwanaland margin: analogy to the middle Proterozoic in North America? *Geology* 17, 324–328.
- Kinny, P.D., Maas, R., 2003. Lu-Hf and Sm-Nd isotope systems in zircon. In: Hanchar, J.M., Hoskin, P.W.O. (Eds.), *Zircon. Reviews of Mineralogy and Geochemistry*, vol. 53, pp. 327–341.
- Lee, H.Y., Chung, S.L., Lo, C.H., Ji, J.Q., Lee, T.Y., Qian, Q., Zhang, Q., 2009. Eocene Neotethyan slab breakoff in southern Tibet inferred from the Linzizong volcanic record. *Tectonophysics* 477, 20–35.
- Liang, Y.H., Chung, S.L., Liu, D.Y., Xu, Y.C., Wu, F.Y., Yang, J.H., Wang, Y.B., Lo, C.H., 2008. Detrital zircon evidence from Burma for reorganization of the eastern Himalayan river system. *American Journal of Science* 308, 618–638.
- Liu, Y.S., Zong, K.Q., Kelemen, P.B., Gao, S., 2008. Geochemistry and magmatic history of eclogites and ultramafic rocks from the Chinese continental scientific drill hole: subduction and ultrahigh-pressure metamorphism of lower crustal cumulates. *Chemical Geology* 247, 133–153.
- Macpherson, C.G., Dreher, S.T., Thirlwall, M.T., 2006. Adakites without slab melting: high pressure differentiation of island arc magma, Mindanao, the Philippines. *Earth and Planetary Science Letters* 243, 581–593.
- Martin, H., 1986. Effect of steeper Archean geothermal gradient on geochemistry of subduction-zone magmas. *Geology* 14, 753–756.
- Martin, H., 1999. Adakitic magmas: modern analogues of Archean granitoids. *Lithos* 46, 411–429.
- McKenzie, D., 1978. Some remarks on the development of sedimentary basins. *Earth and Planetary Science Letters* 40, 25–32.

- McMillan, N.J., Davidson, J.P., Wörner, G., Harmon, R.S., Moorbath, S., Lopez-Escobar, L., 1993. Influence of crustal thickening on arc magmatism: Nevados de Payachata volcanic region, northern Chile. *Geology* 21, 467–470.
- Meng, F.Y., Zhao, Z.D., Zhu, D.C., Zhang, L.L., Guan, Q., Liu, M., Yu, F., Mo, X.X., 2010. Petrogenesis of Late Cretaceous adakite-like rocks in Mamba from the eastern Gangdese, Tibet. *Acta Petrologica Sinica* 26, 2180–2192.
- Mo, X.X., Dong, G.C., Zhao, Z.D., Guo, T.Y., Wang, L.L., Chen, T., 2005a. Timing of magma mixing in Gangdese magmatic belt during the India–Asia collision: zircon SHRIMP U–Pb dating. *Acta Geologica Sinica* 79, 66–76.
- Mo, X.X., Dong, G.C., Zhao, Z.D., Zhou, S., Wang, L.L., Qiu, R.Z., Zhang, F.Q., 2005b. Spatial and temporal distribution and characteristics of granitoids in the Gangdese, Tibet and implication for crustal growth and evolution (in Chinese with English abstract). *Geological Journal of China Universities* 11, 281–290.
- Mo, X.X., Hou, Z.Q., Niu, Y.L., Dong, G.C., Qu, X.M., Zhao, Z.D., Yang, Z.M., 2007. Mantle contributions to crustal thickening during continental collision: evidence from Cenozoic igneous rocks in southern Tibet. *Lithos* 96, 225–242.
- Mo, X.X., Zhao, Z.D., Deng, J.F., Dong, G.C., Zhou, S., Guo, T.Y., Zhang, S.Q., Wang, L.L., 2003. Response of volcanism to the India–Asia collision. *Earth Science Frontiers* 10, 135–148 (in Chinese with English abstract).
- Murphy, M.A., Yin, A., Harrison, T.M., Dürr, S.B., Chen, Z., Ryerson, F.J., Kidd, W.S.F., Wang, X., Zhou, X., 1997. Did the Indo-Asian collision alone create the Tibetan plateau? *Geology* 25, 719–722.
- Pan, G.T., Ding, J., Yao, D.S., Wang, L.Q., 2004. Guidebook of 1: 1, 500, 000 Geologic Map of the Qinghai–Xizang (Tibet) Plateau and Adjacent Areas, vol. 1–148. Cartographic Publishing House, Chengdu, China.
- Powell, C.M., 1986. Continental underplating model for the rise of the Tibetan plateau. *Earth and Planetary Science Letters* 81, 79–94.
- Powell, C.M., Conaghan, P.J., 1973. Plate tectonics and the Himalaya. *Earth and Planetary Science Letters* 20, 1–12.
- Quidelleur, X., Grove, M., Lovera, O.M., Harrison, T.M., Yin, A., Ryerson, F.J., 1997. The thermal evolution and slip history of the Renbu Zedong Thrust, southeastern Tibet. *Journal of Geophysical Research* 102, 2659–2679.
- Rapp, R.P., Watson, E.B., 1995. Dehydration melting of metabasalt at 8–32 kbar: implications for continental growth and crust–mantle recycling. *Journal of Petrology* 36, 891–931.
- Rapp, R.P., Shimizu, N., Norman, M.D., Applegate, G.S., 1999. Reaction between slab-derived melts and peridotite in the mantle wedge: experimental constraints at 3.8 GPa. *Chemical Geology* 160, 335–356.
- Schärer, U., Xu, R.H., Allègre, C.J., 1984. U–Pb geochronology of Gandese (Transhimalaya) plutonism in the Lhasa–Xigaze region Tibet. *Earth and Planetary Science Letters* 69, 311–320.
- Sheffels, B.M., 1990. Lower bound on the amount of crustal shortening in the central Bolivian Andes. *Geology* 18, 812–815.
- Wen, D.R., Chung, S.L., Song, B., Iizuka, Y., Yang, H.J., Ji, J.Q., Liu, D.Y., Gallet, S., 2008a. Late Cretaceous Gangdese intrusions of adakitic geochemical characteristics, SE Tibet: petrogenesis and tectonic implications. *Lithos* 105, 1–11.
- Wen, D.R., Liu, D.Y., Chung, S.L., Chu, M.F., Ji, J.Q., Zhang, Q., Song, B., Lee, T.Y., Yeh, M.W., Lo, C.H., 2008b. Zircon SHRIMP U–Pb ages of the Gangdese batholith and implications for Neotethyan subduction in southern Tibet. *Chemical Geology* 252, 191–201.
- Wu, F.Y., Huang, B.C., Ye, K., Fang, A.M., 2008. Collapsed Himalayan–Tibetan orogen and the rising Tibetan Plateau. *Acta Petrologica Sinica* 24, 1–30 (in Chinese with English abstract).
- Wu, F.Y., Ji, W.Q., Liu, C.Z., Chung, S.L., 2010. Detrital zircon U–Pb and Hf isotopic data from the Xigaze fore-arc basin: constraints on Transhimalayan magmatic evolution in southern Tibet. *Chemical Geology* 271, 13–25.
- Xie, K.J., Zeng, L.S., Liu, J., Gao, L.E., 2010. Late-Eocene Dala adakitic granite, southern Tibet and geological implications. *Acta Petrologica Sinica* 26, 1016–1026.
- Xie, L.W., Zhang, Y.B., Zhang, H.H., Sun, J.F., Wu, F.Y., 2008. In situ simultaneous determination of trace elements, U–Pb and Lu–Hf isotopes in zircon and baddeleyite. *Chinese Science Bulletin* 53, 1565–1573.
- Xu, J.F., Shinjo, R., Defant, M.J., Wang, Q., Rapp, R.P., 2002. Origin of Mesozoic adakitic intrusive rocks in the Ningzhen area of east China: partial melting of delaminated lower continental crust? *Geology* 30, 1111–1114.
- Xu, R.H., Schärer, U., Allègre, C.J., 1985. Magmatism and metamorphism in the Lhasa block (Tibet): a geochronological study. *Journal of Geology* 93, 41–57.
- Yang, J.S., Xu, Z.Q., Li, Z.L., Xu, X.Z., Li, T.F., Ren, Y.F., Li, H.Q., Chen, S.Y., Robinson, P.T., 2009. Discovery of an eclogite belt in the Lhasa block, Tibet: a new border for Paleo-Tethys? *Journal of Asian Earth Sciences* 34, 76–89.
- Yin, A., Harrison, T.M., 2000. Geologic evolution of the Himalayan Tibetan Orogen. *Annual Review of Earth Planetary Sciences* 28, 211–280.
- Yogodzinski, G.M., Lees, J.M., Churikova, T.G., Dorendorf, F., Wöerner, G., Volynets, O.N., 2001. Geochemical evidence for the melting of subducting oceanic lithosphere at plate edges. *Nature* 409, 500–505.
- Zeng, L.S., Gao, L.E., Xie, K.J., Liu-Zeng, J., 2011. Mid-Eocene high Sr/Y granites in the Northern Himalayan Gneiss Domes: melting thickened lower continental crust. *Earth and Planetary Science Letters* 303, 251–266.
- Zhang, H.F., Xu, W.C., Guo, K.Q., Cai, H.M., Yuan, H.L., 2007. Zircon U–Pb and Hf isotopic composition of deformed granite in the southern margin of the Gangdese belt, Tibet: evidence for early Jurassic subduction of Neo-Tethyan oceanic slab. *Acta Petrologica Sinica* 23, 1347–1353 (in Chinese with English abstract).
- Zhang, Z.M., Zhao, G.C., Santosh, M., Wang, J.L., Dong, X., Shen, K., 2010a. Late Cretaceous charnockite with adakitic affinities from the Gangdese batholith, southeastern Tibet: evidence for Neo-Tethyan mid-ocean ridge subduction? *Gondwana Research* 17, 615–631.
- Zhang, H.F., Harris, N., Guo, L., Xu, W.C., 2010b. The significance of Cenozoic magmatism from the western margin of the eastern syntaxis, southeast Tibet. *Contributions to Mineralogy and Petrology* 160, 83–98.
- Zhao, W.J., Zhao, X., Shi, D.N., Liu, K., Jiang, W., Wu, Z.H., Xiong, J.Y., Zheng, Y.K., 2004. Progress in the study of deep profiles of Tibet and the Himalayas (INDEPTH). *Acta Geologica Sinica* 78, 931–939.
- Zhao, W.L., Morgan, W.J., 1985. Uplift of the Tibetan plateau. *Tectonics* 4, 359–369.
- Zhao, W.L., Morgan, W.J., 1987. Injection of India crust into Tibetan lower crust: a two-dimensional finite element model study. *Tectonics* 6, 489–504.
- Zhu, D.C., Mo, X.X., Niu, Y., Zhao, Z.D., Wang, L.Q., Liu, Y.S., Wu, F.Y., 2009a. Geochemical investigation of Early Cretaceous igneous rocks along an east–west traverse throughout the central Lhasa Terrane, Tibet. *Chemical Geology* 268, 298–312.
- Zhu, D.C., Mo, X.X., Niu, Y.L., Zhao, Z.D., Yang, Y.H., Wang, L.Q., 2009b. Zircon U–Pb dating and in-situ Hf isotopic analysis of Permian peraluminous granite in the Lhasa terrane, southern Tibet: implications for Permian collisional orogeny and paleogeography. *Tectonophysics* 469, 48–60.
- Zhu, D.C., Mo, X.X., Zhao, Z.D., Niu, Y.L., Wang, L.Q., Chu, Q.H., Pan, G.T., Xu, J.F., Zhou, C.Y., 2010. Presence of Permian extension- and arc-type magmatism in southern Tibet: paleogeographic implications. *Geological Society of America Bulletin* 122, 979–993.
- Zhu, D.C., Pan, G.T., Chun, S.L., Liao, Z.L., Wang, L.Q., Li, G.M., 2008. SHRIMP zircon age and geochemical constraints on the origin of Early Jurassic volcanic rocks from the Yeba Formation, southern Gangdese in south Tibet. *International Geology Review* 50, 442–471.
- Zhu, D.C., Pan, G.T., Mo, X.X., Wang, L.Q., Liao, Z.L., Zhao, Z.D., Dong, G.C., Zhou, C.Y., 2006. Late Jurassic–Early Cretaceous geodynamic setting in middle–northern Gangdese: new insights from volcanic rocks. *Acta Petrologica Sinica* 22, 534–546 (in Chinese with English abstract).
- Zhu, D.C., Pan, G.T., Zhao, Z.D., Lee, H.Y., Kang, Z.Q., Liao, Z.L., Wang, L.Q., Li, G.M., Dong, G.C., Liu, B., 2009c. Early Cretaceous subduction-related adakite-like rocks in the Gangdese, south Tibet: products of slab melting and subsequent melt–peridotite interaction? *Journal of Asian Earth Sciences* 34, 298–309.
- Zhu, D.C., Zhao, Z.D., Niu, Y.L., Mo, X.X., Chung, S.L., Hou, Z.Q., Wang, L.Q., Wu, F.Y., 2011. The Lhasa Terrane: record of a microcontinent and its histories of drift and growth. *Earth and Planetary Science Letters* 301, 241–255.